Coexistence of 'α+ ^{208}Pb' cluster structures and single-particle excitations in $^{212}_{84}Po_{128}$

A. Astier[1], P. Petkov[1,2], M.-G. Porquet[1], D.S. Delion[3,4], and P. Schuck[5]
[1] *CSNSM, IN2P3-CNRS and Université Paris-Sud 91405 Orsay, France*
[2] *INRNE, BAS, 1784 Sofia, Bulgaria*
[3] *Horia Hulubei National Institute of Physics and Nuclear Engineering 407 Atomistilor, 077125 Bucharest, Romania*
[4] *Academy of Romanian Scientists, 54 Splaiul Independentei 050094 Bucharest, Romania*
[5] *IPN, IN2P3-CNRS and Université Paris-Sud 91406 Orsay, France*

Excited states in ^{212}Po have been populated by α transfer using the ^{208}Pb(^{18}O, ^{14}C) reaction at 85 MeV beam energy and studied with the EUROBALL IV γ multidetector array. The level scheme has been extended up to $\sim$ 3.2 MeV excitation energy from the triple γ coincidence data. Spin and parity values of most of the observed states have been assigned from the γ angular distributions and $\gamma - \gamma$ angular correlations. Several γ lines with $E_\gamma < 1$ MeV have been found to be shifted by the Doppler effect, allowing for the measurements of the associated lifetimes by the DSAM method. The values, found in the range [0.1-0.6] ps, lead to very enhanced E1 transitions. All the emitting states, which have non-natural parity values, are discussed in terms of α-^{208}Pb structure. They are in the same excitation-energy range as the states issued from shell-model configurations.

PACS numbers: 25.70.Hi, 27.80.+w, 23.20.-g, 21.60.Gx

I. INTRODUCTION

The ^{212}Po nucleus is the last member of the ^{232}Th radioactive chain. As early as 1916, Rutherford and Wood discovered [1] the emission of α particles from the end of this chain, the "active deposit" of thorium (formerly named as ThB). Many years later, this was interpreted as the α decays of several states of ^{212}Po, particularly its ground state which is a pure α emitter, with a very short half-life, 0.299(2) μs. Afterwards new α activities were produced by heavy/light-ion bombardments of bismuth and lead, and their decay spectra were measured [2]. These studies have shown that an α-line at 11.6 MeV arises directly from an isomeric state of ^{212}Po with a half-life of 45 s, i.e. 1.5×10^8 longer than the ground-state one. The very large hindrance factor for this α emission was explained by spin and parity assignments of 18^+ for the ^{212}Po isomeric state, which has been located at 2.9 MeV excitation energy.

Besides these two extreme states, other levels were identified from the β-decay of the two long-lived states of ^{212}Bi or *via* light-ion induced transfer reactions, such as (^{18}O,^{14}C) or (^{9}Be,α n) on a ^{208}Pb target [3, 4], and all the yrast levels were discussed in terms of shell model configurations. The ^{212}Po nucleus has been also studied in neutron-evaporation channels from total-fusion reactions, using either a radioactive target [5], ^{210}Pb(α, 2n), or a radioactive beam [6, 7], ^{208}Pb(^{8}He,4n). However, the limited number of the target nuclei or the projectiles did not sizeably improve the spectroscopic data obtained in the ^{208}Pb(^{9}Be,α n) reaction [4].

There were numerous attempts to give a microscopic description of the α decay of the ground state of ^{212}Po. The use of shell-model configurations fails to reproduce the large value of its rate by an order of magnitude, meaning that the α-particle formation is badly predicted within this approach. When complemented by cluster-model-type basis states [8], the decay width is predicted in good agreement with the experimental value, the amount of α clustering in the ground state of ^{212}Po being $\sim$0.3. This is not far from the high degrees of clustering well known in some light nuclei where the two neutrons and the two protons occupy the same orbit, which is not fulfilled in the present case.

The existence of the α cluster would also act upon the properties of the excited states of ^{212}Po. Whereas shell-model approaches work well to predict the excitation energy of the yrast states [4], they cannot reproduce their large experimental B(E2) transition strengths, which are well accounted for from the α clustering (see for instance refs. [9–12]). All these results point to the fact that the positive-parity yrast states do contain both components, shell-model configurations and α clustering, which are not easy to disentangle.

In this paper, we present a new class of excited states of ^{212}Po, which have non-natural parity and are connected by enhanced E1 transitions to the yrast states. Low-lying shell-model excitations do not lead to such non-natural parity states and these states are the first experimental evidence of "pure" α-cluster states in heavy nuclei. The ^{212}Po nuclei have been obtained using the (^{18}O,^{14}C) transfer reaction on a thick ^{208}Pb target and γ^n measurements have been performed. The experimental conditions and the various analysis techniques are presented in section II. Section III is devoted to the experimental results which comprise *i)* the analysis of the reaction mechanism leading to the ^{212}Po channel, *ii)* the new level scheme of ^{212}Po, *iii)* the lifetime measurements using the Doppler Shift Attenuation Method (DSAM) , and *iv)* the α branching ratios of the yrast states. In the last part

(section IV) we review several properties of the first excited states of ^{212}Po in order to underline the contribution of the α-clustering. Then we discuss the oscillatory motion of the α-core distance which may give rise to non-natural parity states.

A letter highlighting parts of the present study has been recently published [13].

II. EXPERIMENTAL DETAILS

A. Reaction, γ-ray detection and analysis

Excited states in ^{212}Po were populated by α transfer using the ^{18}O+^{208}Pb reaction, the ^{18}O beam with an energy of 85 MeV being provided by the Vivitron tandem of IReS (Strasbourg). A 100 mg/cm^2 self-supporting target of ^{208}Pb was employed, which was thick enough to stop the recoiling ^{212}Po nuclei. It is worth noting that due to this large thickness, the ^{18}O beam was stopped in the Pb target too, and therefore the incident energy covered a large range of values, above and below the Coulomb barrier. The kinematics of the α transfer leading to high-spin states in ^{212}Po in this experiment is detailed below (see sect. III A). The de-exciting γ-rays were recorded with the EUROBALL IV array consisting of 71 Compton-suppressed Ge detectors [14] (15 cluster germanium detectors placed in the backward hemisphere with respect to the beam, 26 clover germanium detectors located around 90°, 30 tapered single-crystal germanium detectors located at forward angles). Each cluster detector is composed of seven closely packed large-volume Ge crystals [15] and each clover detector consists of four smaller Ge crystals [16]. The 239 Ge crystals of the Euroball array could be grouped into 13 rings, with the following angles with respect to the beam axis, 15.5° (5 crystals), 34.6° (10), 52.3° (15), 72.2° (26), 80.9° (26), 99.1° (26), 107.5° (26), 122.6° (10), 130.5° (30), 138.7° (25), 148.1° (15), 155.9° (15), and 163.5° (10), i.e. 3 rings forward, 4 rings close to 90° and 6 rings backward with respect to the beam axis.

Events were recorded on tape when at least 3 unsuppressed Ge detectors fired in prompt coincidence. In this way, a set of $\sim 4\times10^9$ three- and higher-fold events were available for subsequent analysis, but only a small part of these data corresponds to ^{212}Po events. Indeed the main objective of the experiment was actually the study of the fusion-fission channel which leads to the production of the high-spin states of $\sim$ 150 fragments, mainly located on the neutron-rich side of the valley of stability [17]. The ^{212}Po study became itself a goal when it turned out that its main γ lines were strong enough in our data set to be precisely analyzed. We have estimated that the cross section of the exit channel leading to ^{212}Po is $\sim$ 10-20 mb, i.e. $\sim$ 10-20% of the cross section of the fusion-fission channel.

Various procedures have then been used for the offline analysis in order to fully characterize the excited levels of ^{212}Po (excitation energy, spin and parity values, decay modes, and multipole matrix elements). Both multi-gated spectra and three-dimensional 'cubes' have been built and analyzed with the Radware package [18], starting from the known transitions deexciting the yrast states [4].

B. γ angular distributions and γ-γ angular correlations

We have checked whether the reaction mechanism involved here leads to spin alignments of ^{212}Po with respect to the beam axis. Thus we have chosen several yrast transitions which are known to be quadrupole ones with $\Delta I = 2$ (such as the 727, 405, and 357 keV transitions) or dipole ones with $\Delta I = 1$ (such as the 577 keV one). Their angular distributions have been found to be symmetric around 90° (see examples in fig.1), the intensity of the quadrupole transitions being maximum along the beam axis, whereas the one of the dipole transition is maximum at 90°, demonstrating that the spins are aligned in a plane perpendicular to the beam axis. When

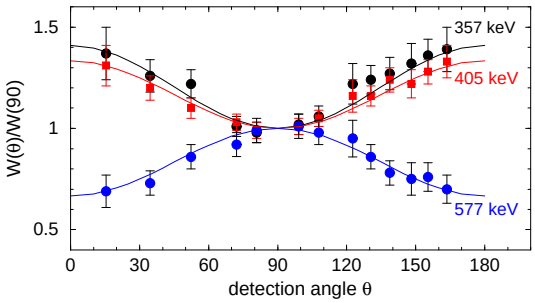

FIG. 1: (color online) Angular distribution of some yrast transitions in the ^{212}Po nucleus produced in the ^{208}Pb(^{18}O,^{14}C) reaction. Solid lines are the fits using the standard Legendre polynomials.

fitted using standard Legendre polynomials $P_{2,4}(cos^2\theta)$, the obtained values of the angular coefficient A_2/A_0 indicate that the alignment is partial, with an attenuation coefficient $\alpha_2 \sim 0.7$ [19].

This allowed us to analyze each gamma-ray angular distribution to determine its multipole order. In order to characterize the transitions having too weak intensity to be analyzed in that way, their anisotropies have been determined using the intensities measured at two angles relative to the beam axis, R_{ADO}=$I_\gamma(39.3°)$/ $I_\gamma(76.6°)$, these two angles being the average angle of the tapered and cluster detectors in the one hand, and the average angle of the clover detectors in the other hand, when taking into account the symmetry of the distribution around 90°. Assuming the same attenuation coefficient as mentioned above ($\alpha_2 \sim 0.7$) theoretical ADO ratios of 0.85 and 1.30 are expected for pure stretched dipole and quadrupole transitions, respectively.

The analysis of γ-γ angular correlations of the most intense transitions has been also performed, in order to get rid of the spin alignment process. For that purpose, the coincidence rates of two successive γ transitions are analyzed as a function of Θ, the average relative angle between the two fired detectors. The Euroball IV spectrometer had $C^2_{239} = 28441$ combinations of 2 crystals, out of which only ~ 2000 involved different values of relative angle within 2°. Therefore, in order to keep reasonable numbers of counts, all the angles (taking into account the symmetry around 90°) have been gathered around three average relative angles : 22°, 46°, and 75° .

The coincidence rate is increasing between 0° and 90° for the dipole-quadrupole cascades, whereas it decreases for the quadrupole-quadrupole or dipole-dipole ones. More precisely, the angular correlation functions at the three angles of interest were calculated for several combinations of spin sequences (see table I), corresponding to typical multipole orders (quadrupole, dipole) and typical spin changes ($\Delta I = 2, 1, 0$). In order to check the method, angular correlations of transitions belonging to the yrast cascades of the fission fragments produced in this experiment and having well-known multipole orders were analyzed and the expected values were found in all cases [20].

TABLE I: Values of the angular correlation functions expected for several combinations of spin values, normalized to the ones calculated at 75°: For each $I_1 \to I_2 \to I_3$ sequence given in the first column, the spin changes due to the two consecutive transitions are given in the second column.

$I_1 \to I_2 \to I_3$ sequence	ΔI values	R(22°)	R(46°)	R(75°)
6-6-4	0-2	1.23	1.12	1.00
6-4-2	2-2	1.13	1.06	1.00
5-4-3	1-1	1.06	1.03	1.00
5-4-2	1-2	0.92	0.96	1.00
7-6-6	1-0	0.91	0.95	1.00

C. Linear polarization

Linear polarization can be measured by the use of segmented detectors acting as a Compton polarimeter, such as the clover detectors of the Euroball IV array [21]. We have performed such an analysis and have confirmed that the three most intense transitions of ^{212}Po have an electric nature. Unfortunately the analysis of the transitions with weaker intensity (even those belonging to the yrast band) could not be done. While single-gated spectra are useless because of the large background, the statistics of the peaks in the double-gated clover spectra are too low to precisely measure the effect we are looking for (the counts in the 'Vertical' and the 'Horizontal' spectra have to differ by less than 10%). We have to stress that in this experiment, the major part of the γ-rays are emitted by the fragments of the fusion-fission exit channel, the summed multiplicity of their γ-ray cascades being around 20. On the other hand, the ^{212}Po exit channel has a low γ-multiplicity. Such a situation is not as favourable as that of a rotational structure typically studied in a fusion-evaporation reaction, even weakly populated, since the high folds of their events strongly enhance the statistics of the multi-gated spectra.

D. Lifetime measurements

The stopping time of ^{212}Po in the Pb target is about one picosecond, thus it would have been expected that all the transitions lying in the low-energy part of the level scheme are emitted at rest. Nevertheless we have found several γ-rays with $E_\gamma < 1$ MeV which exhibit shifts and broadenings in energy due to the Doppler effect, meaning that they are emitted in flight and thus the corresponding excited states do have lifetimes shorter than 1 ps.

The lifetime determination using the Doppler-shift attenuation method (DSAM) is based on the time-correlation between the slowing-down of the recoiling ion and the decay of the nuclear level of interest (cf. e.g. ref. [22]). At a fixed direction of observation, e.g. at an angle θ with respect to the beam axis, the spectrum (line-shape) of the registered γ-rays is given, because of the relation $E^{Sh}_\gamma = E_{\gamma_0}(1 + v_\theta/c)$, by the following formula:

$$S_{ij}(E_\gamma) = b_{ij} \int_{-\infty}^{\infty} dE^{Sh}_\gamma \Phi(E_\gamma, E^{Sh}_\gamma) \int_0^\infty dt P_\theta(t, v_\theta) \lambda_i n_i(t) \quad (1)$$

Here, v_θ is the velocity projection on the observation axis, the function $n_i(t)$ represents the time-dependent population of the level i, λ_i is its decay constant and b_{ij} is the branching of the de-exciting transition $i \to j$. The recorded γ-ray spectrum is obtained by a convolution (folding) with the response function Φ of the detector. The quantity $P_\theta(t, v_\theta)$ is the stopping matrix which represents the normalized distributions of the velocity projection v_θ at different times t. Depending on the experimental situation, additional corrections for geometry, efficiency, angular correlation and kinematics effects (cf. ref. [22]) have also to be taken into account in Eq. 1. To reproduce the line-shape and derive the lifetime, it is necessary to correctly determine $P_\theta(t, v_\theta)$, which describes the stopping process, and to solve Eq. 1 with respect to the decay function $\lambda_i n_i(t)$ of the level of interest i. Thereby, the influence of the feeding i.e. of the cascade history has also to be considered.

For the description of the slowing-down process via Monte-Carlo methods (i.e. for the calculation of the matrix $P_\theta(t, v_\theta)$) we used a modified version of the computer code DESASTOP [23, 24] by G. Winter (cf. also ref .[25]).

III. EXPERIMENTAL RESULTS

A. Kinematics of the reaction

The Doppler effect, if any, can be used to determine the direction and the modulus of the velocity of the recoiling nuclei produced in the reaction. Fortunately, the 780 keV transition, located in the high-energy part of the level scheme (this is discussed below, see sect. III B), displays only shifted components. This can be seen in the triple gated spectrum drawn in figure 2. The 780 keV transition is shifted and broadened by the Doppler effect, whereas the 727 keV ($2^+ \rightarrow 0^+$) transition is emitted by a fully stopped nucleus. We have precisely measured the energy

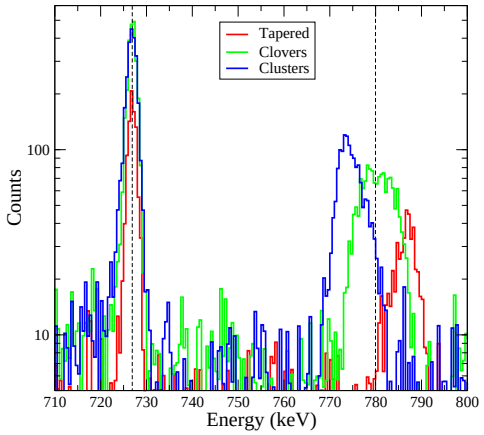

FIG. 2: (color online) Parts of typical triple-gated spectra as a function of the detection angles -tapered Ge (forward angles), clover Ge (around 90°) and cluster Ge (backward angles)- emphasizing the Doppler shift and broadening of the 780 keV transition, whereas the energy and the width of the 727 keV line do not depend on the detection angle. The two dashed lines indicate the 727.1 keV and 780.4 keV energies.

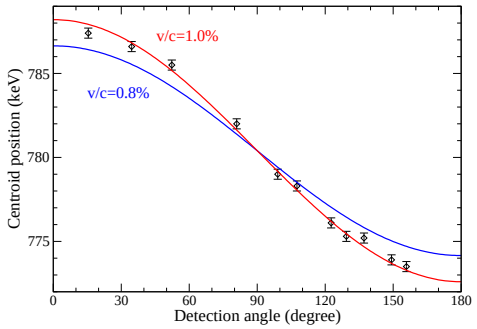

FIG. 3: (color online) Energy of the Doppler-shifted line around 780 keV as a function of the detection angle. The red curve is the best fit obtained for a relative velocity $\frac{v}{c}$=1% and a transition energy of 780.4 keV. The blue curve corresponds to the velocity of the ^{226}Th compound nucleus, $\frac{v}{c}$=0.8%.

of the 780 keV transition as a function of the detector angle, the results are displayed in fig. 3. The symmetry around 90° implies that the ^{212}Po nuclei recoil along the beam axis. The best fit gives $\frac{v}{c}$=1% and a transition energy of 780.4 keV.

The direction and the modulus of this velocity indicate that the ^{14}C ejectiles are also emitted along the beam axis, but in the backward direction[1], which is in perfect agreement with previous results. Many years ago, transfer reactions induced by ^{16}O on ^{208}Pb have been studied [26] in the energy range of 77 to 102 MeV, the scattered particles being identified using Si telescopes and their angular distribution measured in interval of 5-10° over the angular range of 30° to 160° in the laboratory system. The results are typical of a grazing collision, showing an energy dependence of the maximum of the distribution, which moves from 60° for 102 MeV incident beam to more than 160° for 80 MeV. Some years later, using the transfer reaction ^{208}Pb(^{18}O, ^{14}C) at bombarding energies below 80 MeV [3], the first excited states of ^{212}Po have been identified from the coincidences between backscattered ejectiles (within an angular range of 151° $\leq \theta_{lab} \leq$ 166°) and γ-rays.

B. Level scheme of ^{212}Po

We fully agree with the results previously obtained on the level scheme of ^{212}Po [4, 6, 7], confirming both the identified γ-rays and their placement in the level scheme. Moreover we have assigned about 50 new γ-rays to ^{212}Po, de-exciting 35 new excited states, about ten of which are located above 2.92 MeV, the energy of its (18^+) long-lived state.

Typical coincidence spectra of ^{212}Po are presented in figure 4. By requiring two conditions among the three most intense lines (727, 405 and 223 keV), almost all transitions of ^{212}Po can be seen, the most intense ones are labeled in figure 4a. The 810 keV transition is located just above the 727 keV level line and cannot be seen in this spectrum. The spectrum of γ-rays in double coincidence with the 727 keV and 810 keV transitions (see figure 4b) shows the transitions belonging to the part of level scheme lying above the 810 keV transition. The three last spectra displayed in figures 4c, 4d and 4e have been obtained by triple gating on three transitions of ^{212}Po, showing different parts of the level scheme which are well populated by the reaction used in this work. In the spectrum gated by two transitions of the yrast band and by the 432 keV line, one can even notice the Doppler-broadened 780 keV transition, which has allowed us to extract the velocity of the recoiling nuclei (see section III A).

[1] If the ^{14}C ejectiles were emitted forward, the velocity of ^{212}Po would be smaller than the velocity of ^{226}Th, the compound nucleus of the ^{18}O+^{208}Pb complete fusion, i.e. 0.8%.

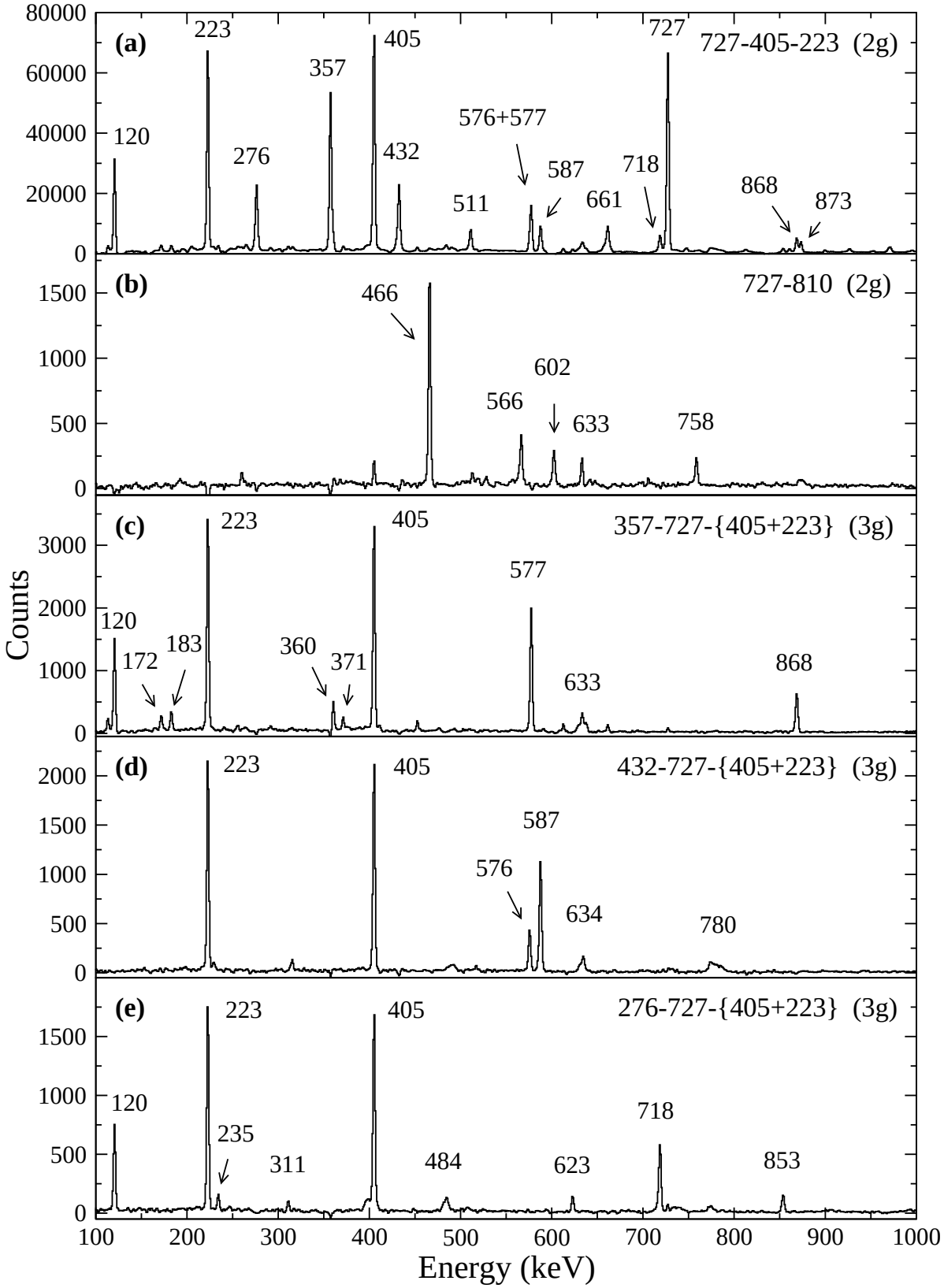

FIG. 4: Background subtracted ^{212}Po spectra built from the following γ-coincidence conditions: (a) 2 gates among 727, 405 and 223 keV; (b) 2 gates: 727 and 810 keV; (c) 3 gates: 357, 727 and (405 or 223) keV; (d) 3 gates: 432, 727 and (405 or 223) keV; (e) 3 gates: 276, 727 and (405 or 223) keV.

All the γ-rays observed in the reaction ^{208}Pb(^{18}O, ^{14}C) are reported in table II, including their relative intensity,

the value of their anisotropy, R_{ADO}=$I_\gamma(39.3°)/ I_\gamma(76.6°)$ and their location in the level scheme. Results of the angular distributions and of angular correlations for the most intense γ-rays are given in tables III and IV. Values of conversion coefficients for the low-energy transitions extracted from total intensity balances done on some selected gated spectra are given in table V, in comparison with theoretical values [27].

The main feature of the level scheme of ^{212}Po obtained in the present work is the rather low multiplicity of the γ cascades, meaning that the α transfer reaction induced by ^{18}O at a bombarding energy close to the Coulomb barrier does not provide so much angular momenta. The new

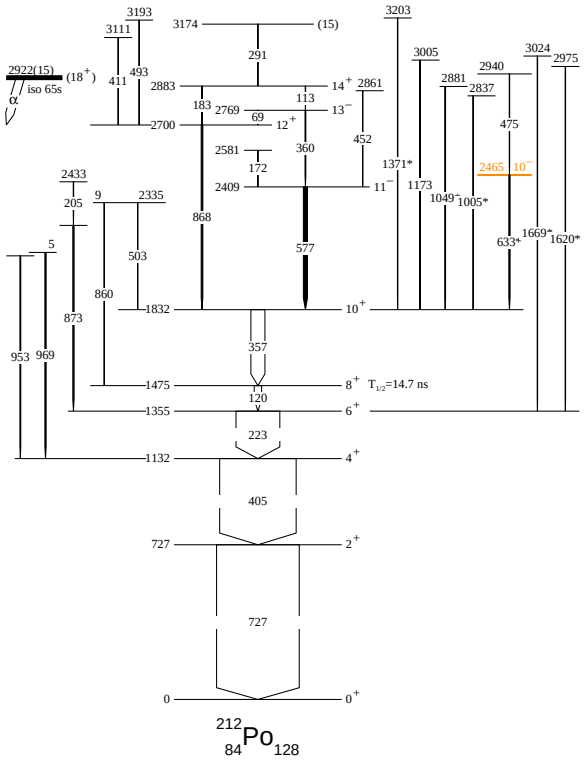

FIG. 5: (color online) First part of the level scheme of ^{212}Po determined in this work, showing the yrast part and levels only linked to yrast states. The long-lived isomeric state at 2922(15) keV excitation energy [28], a pure α-emitter not observed in the present work, is drawn for the sake of completeness. The half-life of the 8^+ yrast state is 14.7(3) ns (see text). The width of the arrows is representative of the intensity of the γ-rays. The transitions marked with an asterisk exhibit Doppler shifts (see sect. III D). The colored state is also displayed in fig. 11.

states which have been identified are lying in a medium range of excitation energy (2.5 MeV-3.2 MeV) and angular momentum ($6\hbar$-$8\hbar$). For the purpose of clarity, the level scheme has been split in two almost independent parts which are displayed in figures 5 and 6.

The first part of the level scheme (see fig. 5) shows the yrast states and the levels only linked to yrast states. We have extended the yrast cascade by only one transition, 291 keV, whereas many new γ-rays have been found to populate directly the lower-spin yrast states, some of them having a high energy. It is worth pointing out that both the 1620 keV and 1669 keV transitions are seen in coincidence with the 727 keV, 405 keV and 223 keV transitions, while their possible coincidence with the 120 keV line could be too lowered because of its very low γ intensity. We have chosen to place the two high-energy transitions directly above the 1335 keV state, but their location above the 1475 keV state cannot be excluded. The spin and parity values of all the yrast states are now determined unambiguously up to the 2883 keV level with I^π=14^+, on the basis of our results for angular distributions (table III), angular correlations (table IV), ADO ratios (table II), as well as the internal conversion electron coefficients of the low-energy transitions (table V). Because of the E1 multipolarity of the 69 keV and the 113 keV transitions, the negative parity of the 2409 keV and the 2769 keV states is now clearly established.

The timing information from the germanium detectors have been used to measure the half-life of the 8^+ yrast state. The procedures were checked using the delayed coincidences of isomeric states of various nuclei produced in this experiment, as described in ref. [20]. The time distribution between the emission of γ-rays located above the 1475 keV level and those below it gives $T_{1/2}$ = 14(1) ns. This is lower than the value obtained in ref. [4], which has been adopted in the ENSDF data base [28]. On this other hand, our value is in better agreement with the two previous results [3, 40], $T_{1/2}$ = 14.2(24) ns and $T_{1/2}$ = 14.7(3) ns, respectively. Then, we select the most accurate value, as shown in fig. 5.

The second part of the level scheme (see fig. 6) shows several groups of excited states linked together and to the yrast states. Some levels display several decay paths which limit the spin values which can be assigned to the involved levels. For instance, the angular distribution results for the 810 keV, 971 keV and 1020 keV transitions (see tables II and III) indicate that they are dipole transitions linking states with $\Delta I = 1$. Thus the spin values of the 1537 keV, 2103 keV and 2374 keV states are 3, 5, and 7, respectively, because of their other decay observed towards the yrast state having one unit more angular momentum (see fig. 6). Knowing that the 587 keV, 359 keV, and 623 keV transitions are dipole transitions linking states with ΔI = 1, the spin values of the 1787 keV, 2016 keV states are *even*. As for the 432 keV transition linking two levels having an even-I value, it could be assigned quadrupole transition with $\Delta I = 2$, as its a_2 angular coefficient is +0.27(7) (see table III), or its coincidence rate with the 223 keV transition is maximum at 22° (see table IV). Nevertheless the I^π value of the 1787 keV state cannot be 8^+, because of its link to the 2103 keV state ($I = 5$) by means of the 315 keV transition. It is worth recalling that a *pure* dipole $\Delta I = 0$ transition has almost identical angular distribution/angular correlations as a quadrupole $\Delta I = 2$ one. Thus the spin

TABLE II: γ-ray transition energies (E_γ), relative γ intensities (I_γ), angular distribution ratios (R_{ADO}), and level and spin assignments for the ^{212}Po nucleus.

$E_\gamma^{(a)}$ (keV)	$I_\gamma^{(b)}$	R_{ADO}	E_i (keV)	E_f (keV)	I_i^π	I_f^π	$E_\gamma^{(a)}$ (keV)	$I_\gamma^{(b)}$	R_{ADO}	E_i (keV)	E_f (keV)	I_i^π	I_f^π
69.2	6(3)		2769.4	2700.4	13^-	12^+	566.3	14(3)	1.32(14)	2102.9	1536.8	$5^{(-)}$	$3^{(-)}$
113.3	3(1)		2882.8	2769.4	14^+	13^-	575.6	10(3)	1.15(8)	2362.7	1786.9	6	6^-
120.3	90(10)	1.28(18)	1474.9	1354.6	8^+	6^+	577.1	49(7)	0.82(2)	2409.1	1832.0	11^-	10^+
157.2	4(2)		2102.9	1945.6	$5^{(-)}$	4^-	587.5	29(5)	0.80(4)	2374.2	1786.9	$7^{(-)}$	6^-
171.7	5(2)		2580.8	2409.1		11^-	601.9	9(3)	0.89(15)	2604.4	2002.5	5	$4^{(-)}$
182.6	5(2)	1.37(16)	2882.8	2700.4	14^+	12^+	612.3*	27(5)	1.24(27)	1744.3	1132.0	4^-	4^+
205.1	5(2)		2432.8	2227.7		7	622.6	3(1)	0.78(10)	2374.2	1751.0	$7^{(-)}$	8^-
222.6	530(30)	1.21(3)	1354.6	1132.0	6^+	4^+	633.2	9(3)	0.82(13)	2170.0	1536.8		$3^{(-)}$
229.8	3(1)		2604.3	2374.2		$7^{(-)}$	633.3*	15(3)	1.20(16)	2465.3	1832.0	10^-	10^+
234.6	4(2)	1.16(13)	1985.7	1751.0	$8^{(-)}$	8^-	633.6	9(3)		2420.5	1786.9		6^-
249.7	3(1)		2235.5	1985.7		$8^{(-)}$	637.3	2(1)		2469.6	1832.0	$9^{(-)}$	10^+
255.2	2(1)		3035.3	2780.2		10	661.3*	51(7)	1.19(9)	2015.9	1354.6	6^-	6^+
259.6	5(2)		2362.7	2102.9	6	$5^{(-)}$	718.4	20(5)	0.76(4)	2469.6	1751.0	$9^{(-)}$	8^-
264.7	7(2)	0.99(9)	2280.7	2015.9		6^-	727.1	–	1.14(2)	727.1	0.0	2^+	0^+
276.1*	58(10)	1.28(7)	1751.0	1474.9	8^-	8^+	740.2*	7(3)		3209.8	2469.6		$9^{(-)}$
291.4	3(2)		3174.2	2882.8	(15)	14^+	748.1	6(3)		2102.9	1354.6	$5^{(-)}$	6^+
310.8	3(2)		2780.2	2469.6	10	$9^{(-)}$	757.2*	8(3)		2860.1	2102.9		$5^{(-)}$
315.5	3(2)		2102.9	1786.9	$5^{(-)}$	6^-	758.4	10(3)	1.15(11)	2295.2	1536.8		$3^{(-)}$
357.1	170(20)	1.26(3)	1832.0	1474.9	10^+	8^+	774	2(1)		2525.0	1751.0		8^-
358.5	11(3)		2102.9	1744.3	$5^{(-)}$	4^-	780.4*	23(5)	1.34(9)	3154.7	2374.2	$7^{(+)}$	$7^{(-)}$
358.6	11(3)	0.85(10)	2374.2	2015.9	$7^{(-)}$	6^-	809.7	76(10)	0.83(6)	1536.8	727.1	$3^{(-)}$	2^+
360.2	10(3)	1.26(15)	2769.4	2409.1	13^-	11^-	813.6*	34(5)	1.13(8)	1945.6	1132.0	4^-	4^+
371.0	3(1)		2780.2	2409.1	10	11^-	853.4	7(2)	0.98(20)	2604.3	1751.0		8^-
397.7*	9(3)		2867.3	2469.6		$9^{(-)}$	860.3	5(2)	0.74(15)	2335.1	1474.9	9	8^+
404.9	924(25)	1.19(2)	1132.0	727.1	4^+	2^+	868.4	19(4)	1.18(6)	2700.4	1832.0	12^+	10^+
405	6(3)		1536.8	1132.0	$3^{(-)}$	4^+	873.1	14(3)	0.84(5)	2227.7	1354.6	7	6^+
406.6*	2(1)		3010.9	2604.3			875.0	4(2)		2877.5	2002.5		$4^{(-)}$
410.7	2(1)	1.08(16)	3111.1	2700.4		12^+	899.0	4(2)		2374.2	1474.9	$7^{(-)}$	6^+
432.3*	75(10)	1.22(6)	1786.9	1354.6	6^-	6^+	926.2	6(3)	0.67(14)	2280.7	1354.6		6^+
452.3	4(2)		2861.4	2409.1		11^-	953.1	8(3)	1.13(29)	2085.1	1132.0		4^+
465.7	50(5)	0.89(9)	2002.5	1536.8	$4^{(-)}$	$3^{(-)}$	968.9	14(3)	0.86(10)	2100.9	1132.0	5	4^+
474.9	3(1)		2940.2	2465.3		10^-	971.1	26(5)	0.79(7)	2102.9	1132.0	$5^{(-)}$	4^+
483.7	4(2)		2469.6	1985.7	$9^{(-)}$	$8^{(-)}$	994.9	4(2)		2469.6	1474.9	$9^{(-)}$	8^+
484.5	7(3)		2235.5	1751.0		8^-	1005*	6(3)		2837	1832.0		10^+
490.2*	5(2)	1.26(15)	2864.5	2374.2	$7^{(+)}$	$7^{(-)}$	1020	8(2)	0.76(7)	2374.2	1354.6	$7^{(-)}$	6^+
492.8	2(1)		3193.2	2700.4		12^+	1049*	9(3)	1.03(17)	2881	1832.0		10^+
502.9	3(1)		2335.1	1832.0	9	10^+	1172.7	2(1)		3004.7	1832.0		10^+
510.9	26(5)	1.10(9)	1985.7	1474.9	$8^{(-)}$	8^+	1371*	6(3)	1.16(20)	3203	1832.0		10^+
518.4	3(1)		2880.9	2362.7		6	1620*	6(3)		2975	1354.6		6^+
563.8*	10(3)		2666.7	2102.9		$5^{(-)}$	1669*	5(2)		3024	1354.6		6^+

[a] Uncertainties in transition energies are typically between 0.1 and 0.5 keV. Transitions showing Doppler shift and broadening are marked by an asterisk, their energy uncertainty can be larger (up to 2 keV).

[b] Intensities measured in this experiment (i.e. with the requirement that a minimum of three unsuppressed Ge detectors fired in prompt coincidence) are normalized to the sum of the values of the two transitions populating the 2_1^+ state, $I_\gamma(404.9\text{ keV}) + I_\gamma(809.7\text{ keV}) = 1000$.

value of the 1787 keV state is fixed to 6. Four other γ-rays drawn in fig. 6 (276 keV, 612 keV, 661 keV, and 814 keV) share the same features as the 432 keV transition. They exhibit Doppler shifts, they are located just above an yrast state, their angular properties indicate that they can be either quadrupole transitions linking states with $\Delta I = 2$ or *pure* dipole transitions linking states with $\Delta I = 0$. Thus we adopt the same conclusion for all these transitions, they are dipole transitions linking states with $\Delta I = 0$, in agreement with the other decay paths of the states located above them. The negative parity of the 1744 keV, 1751 keV, 1787 keV, 1946 keV, and 2016 keV

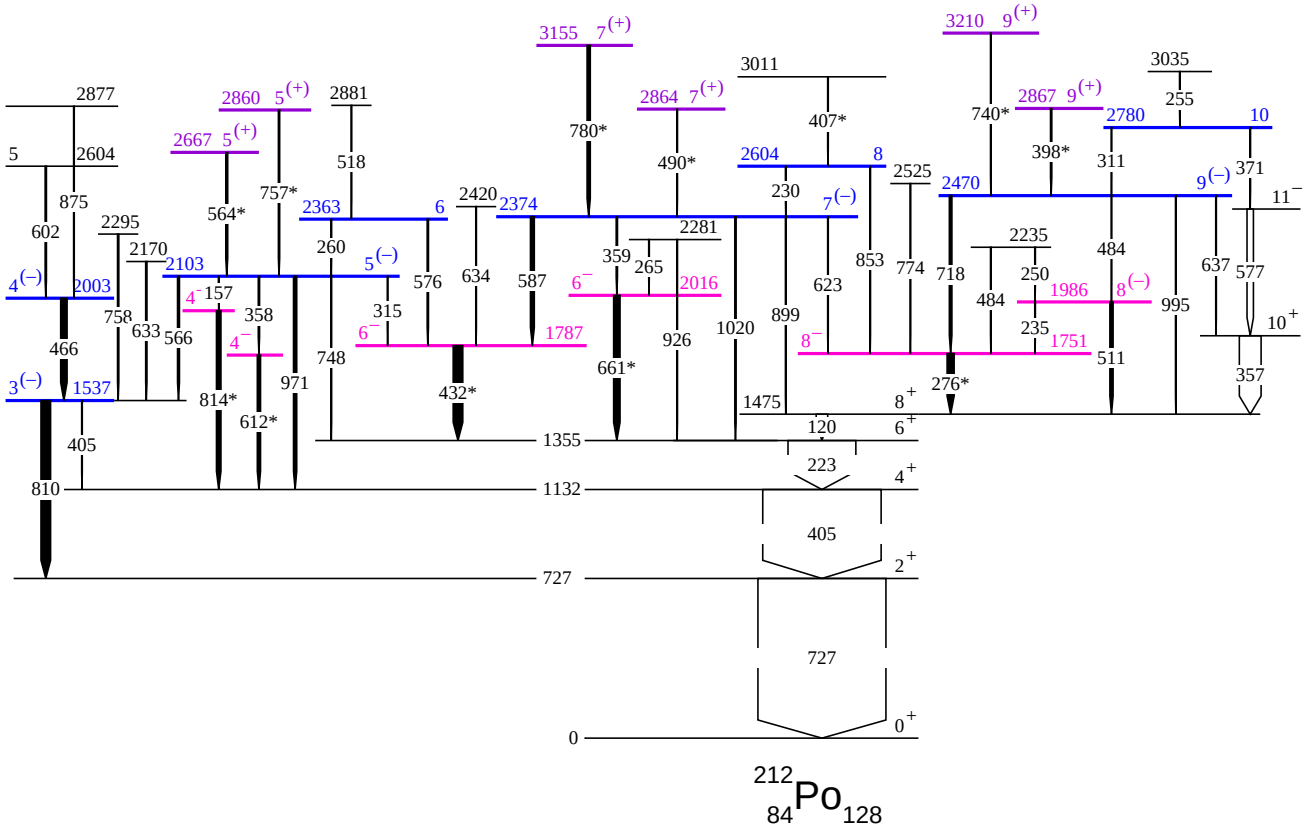

FIG. 6: (color online) Second part of the level scheme of ^{212}Po determined in this work, showing several groups of excited states linked together and to the yrast states. The width of the arrows is representative of the intensity of the γ-rays. The transitions marked with an asterisk exhibit Doppler shifts (see sect. III D). The colored states are also displayed in fig. 11.

TABLE III: Angular distribution coefficient (a_2) and multipole order of the most intense γ-rays of ^{212}Po. The transitions marked with an asterisk are discussed in sects. III C and III D.

E_γ	$a_2^{(a)}$	multipole order	spin sequence$^{(b)}$
727.1	+0.16(4)	ΔI=2 quadrupole	$2^+ \rightarrow 0^+$
404.9	+0.20(4)	ΔI=2 quadrupole	$4^+ \rightarrow 2^+$
222.6	+0.18(3)	ΔI=2 quadrupole	$6^+ \rightarrow 4^+$
357.1	+0.24(4)	ΔI=2 quadrupole	$10^+ \rightarrow 8^+$
577.1	−0.25(5)	ΔI=1 dipole	$11^- \rightarrow 10^+$
868.4	+0.18(6)	ΔI=2 quadrupole	$12^+ \rightarrow 10^+$
276.1*	+0.29(6)	ΔI=0 dipole	$8^- \rightarrow 8^+$
432.3*	+0.27(7)	ΔI=0 dipole	$6^- \rightarrow 6^+$
465.7	−0.5(1)	ΔI=1 dipole	$4^{(-)} \rightarrow 3^{(-)}$
575.6	+0.3(1)	ΔI=0 dipole	$6 \rightarrow 6^-$
587.5	−0.23(8)	ΔI=1 dipole	$7^{(-)} \rightarrow 6^-$
661.3*	+0.26(9)	ΔI=0 dipole	$6^- \rightarrow 6^+$
718.4	−0.29(5)	ΔI=1 dipole	$9^{(-)} \rightarrow 8^-$
1020	−0.28(8)	ΔI=1 dipole	$7^{(-)} \rightarrow 6^+$

$^{(a)}$ The number in parenthesis is the error in the last digit.
$^{(b)}$ see text.

states will be discussed in the next section.

TABLE IV: Coincidence rates between γ-rays of ^{212}Po as a function of their relative angle of detection, normalized to the ones obtained around 75°.

E_γ-E_γ	R(22°)	R(46°)	R(75°)
405 - 727	1.10(4)	1.06(2)	1.00(1)
223 - 405	1.10(3)	1.05(2)	1.00(1)
577 - 357	0.89(5)	0.97(4)	1.00(3)
223 - 276	1.12(6)	1.09(4)	1.00(2)
223 - 432	1.15(6)	1.12(4)	1.00(3)
223 - 661	1.22(7)	1.08(5)	1.00(3)

Due to coincidence relationships and/or spin values, we propose two different states at 2604 keV, one deexcites towards the 2003 keV state by means of the 602 keV transition, while the second one is linked to the 2374 keV state and to the 1751 keV one (see fig. 6). Secondly, two transitions at 968.9-971.1 keV deexcite two states close in energy (2100.9-2102.9 keV). Both members of the doublet, being clearly seen in coincidence with the two first yrast transitions, are located just above the 1132.0 keV level (see figs. 5 and 6). Whereas there is no other transition in coincidence with the lower-energy member, the

TABLE V: Conversion coefficients for the low-energy transitions of ^{212}Po extracted from intensity balances done on gated spectra, the theoretical values come from the *BrIcc* database [27]. The transitions marked with an asterisk are discussed in sects. III C and III D.

E (keV)		α (exp)	α (E1)	α (E2)	α (M1)	adopted
69.2	tot	0.2(1)	0.26	39.2	6.2	E1
113.3	tot	< 3.0	0.33	4.26	7.77	E1
120.3	tot	3.2(5)	0.29	3.32	6.60	E2
	K			0.41		
182.6	tot	0.6(3)	0.10	0.65	2.00	E2
222.6	tot	0.33(5)	0.063	0.33	1.15	E2
	K			0.13		
276.1*	tot	0.37(7)	0.038	0.162	0.635	E1$^{(a)}$
	K	~ 0.4	0.031	0.081	0.516	
432.3*	tot	0.13(3)	0.014	0.046	0.188	E1$^{(a)}$
	K	~ 0.1	0.011	0.030	0.153	

$^{(a)}$ see sect. III C

higher-energy member exhibits the same coincidence relationships as the 566 keV transition (see fig. 6). Lastly, we have assumed that there is only one level at 2335 keV (deexcited by 861 and 503 keV transitions, see fig. 5), as well as only one level at 2281 keV (deexcited by the 265 keV and 926 keV transitions, see fig. 6) and one level at 2235 keV (deexcited by the 250 keV and 484 keV transitions) but we could not strengthen these three hypotheses because of lack of coincidence relationships.

C. Anomalous conversion coefficients of the 276 keV and 432 keV transitions

We have extracted the internal conversion electron coefficients of some transitions of ^{212}Po by analyzing the relative intensities of transitions in cascade. The intensity imbalances of the 120.3 keV and the 222.6 keV transitions measured in spectra in double coincidence with at least one γ-ray located above them lead to α_{tot}(120 keV)=3.3(4) and α_{tot}(223 keV)=0.33(4), in good agreement with the theoretical values for E2 multipolarity [27]. In addition (see table V), we have found α_{tot}(276 keV)=0.37(7) and α_{tot}(432 keV)=0.13(3).

The vacancies in the K electron shell due to the emission of an internal conversion electron lead to X-ray emission and conversely the rate of X-rays emitted in any cascade is correlated to the α_K values of the involved transitions. We have exploited this feature to measure some α_K coefficients. For instance, in the spectra in double coincidence with the 79 keV K_{α_1} X-ray of Po and the 577 keV (or 357 keV) transition, the loss in intensity of the 120 keV transition is three times higher than the one of the 223 keV transition, in agreement with the ratio of their α_K coefficient [27]. In the spectrum in double coincidence with the 587 keV γ-ray and the 79 keV X-ray, the 432 keV transition exhibits the same drop in intensity as the 223 keV one (compare the A1 and A2 spectra of fig. 7). Thus we obtain α_K(432 keV) $\approx \alpha_K$(223 keV, E2)(= 0.13). In the same way (see the B1 and B2 spectra of fig. 7), we get α_K(276 keV) $\approx \alpha_K$(120 keV, E2)(= 0.41).

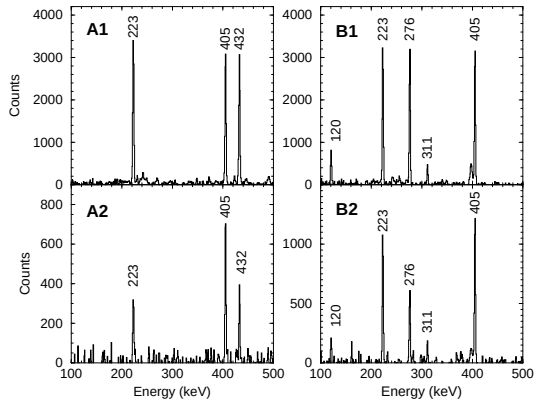

FIG. 7: **Left**: spectra of γ-rays in double coincidence with the 587 keV and 727 keV transitions (A1) and with the 587 keV and 79 keV (K_{α_1} X-ray of Po) transitions (A2). **Right**: spectra of γ-rays in double coincidence with the 718 keV and 727 keV transitions (B1) and with the 718 keV and 79 keV transitions (B2).

The multipolarities of the 276 keV and 432 keV transitions derived from their α_{tot} values could be M1+E2, implying a mixing $\delta^2 \sim 1$, *i.e.* 50% M1 + 50% E2. However, the occurrence of such a very large E2 component leads to major discrepancies:

- The a_2 angular coefficient computed for such mixed multipolarities is no longer in agreement with the measured values, as the quadrupole component leads to a large decrease of the a_2 coefficient (for δ=+1) and even to a quasi-isotropic emission (for δ=-1).
- The B(E2) reduced transition probability computed from the lifetime of the 1751 keV state (given in the next section) largely exceeds the recommended upper limit (RUL) for γ-ray strengths: B(E2, 276 keV) $\sim 5 \times 10^3$ *W.u.*, that is larger than what is obtained for E2 transitions *inside* the superdeformed bands in the Hg-Pb region, B(E2, SD) $\sim 2 \times 10^3$ *W.u.*.

It is noteworthy that the E2 component of the 432 keV transition would lead to B(E2) $\sim 6 \times 10^2$ *W.u.*. Such a large value would be the sign of a quadrupole deformation, implying a rotational behaviour, contrary to what is observed (the 120 keV transition populating the same yrast state as the 432 keV transition has B(E2) ~ 10 *W.u.*, see fig. 13).

As well, the E1+M2 multipolarity that could account for the two α_{tot} values ($\sim$ 15–20% M2) cannot be adopted

because of the tremendous values of the B(M2) reduced transition probabilities calculated using the lifetimes of the states (given in the next section).

Thus we conclude that these transitions must have a pure E1 multipolarity, with *anomalous* conversion coefficients. In the theoretical calculations of the conversion coefficients such as those of ref. [27], the nucleus is assumed to be a homogeneously charged *sphere*, i.e. without any electromagnetic moment, and the electron remains outside the nucleus. Nevertheless, it is well known that the atomic electrons can penetrate within the nuclear charge and current distributions, giving additional nuclear matrix elements into the expression for the rate of internal-conversion-electron ejection [29]. Then the conversion coefficients may have *anomalous* values depending on nuclear structure [30, 31]. Furthermore, the nuclear electromagnetic moments add several coupling terms to the Dirac equation of the electron [32]. Altogether, these effects should largely shift the values of the conversion coefficients of the 276 keV and 432 keV transitions since they are emitted by peculiar states having a very large dipole moment, as outlined later (see sect. IV D).

As a result, the 1751 keV and 1787 keV states have a negative parity and we adopt the same conclusion for the 1744 keV, 1946 keV, and 2016 keV states since their decaying γ-rays share the same features as the 276 keV and 432 keV transitions, as above mentioned. The negative parity of these five states accounts for their unique decay to the yrast state having the same I value[2].

D. Lifetime measurements

As introduced previously, several γ-rays in ^{212}Po exhibit Doppler shifts. A total of 18 transitions have been found to display this feature (they are marked with an asterisk in table II), implying that 18 excited states do have shorter lifetimes than the stopping time of ^{212}Po in the lead target.

Seven lines – namely the 276 keV, 432 keV, 612 keV, 633 keV, 661 keV, 780 keV and 814 keV transitions – deexciting some of those states, could be analyzed to get the lifetime using the Doppler-shift attenuation method (DSAM), whereas in two cases (490 keV and 1049 keV transitions), only a limit of the value could be obtained. As for the 9 last cases, the statistics was too low to perform any analysis and the lifetimes for the corresponding levels are assumed to be smaller than 1.4 ps, the mean value of the stopping time of the ^{212}Po recoils (reported below).

[2] In case of positive parity, we would have to understand why these five states do not decay to the $(I-2)$ yrast states. For instance, the E2 decay of the 1787 keV state to the 4^+ yrast state at 1132 keV would be enhanced because of its energy by a factor of 8 as compared to the one to the 6^+ yrast state.

The kinematics of the quasi-elastic transfer reaction was taken into account and fine tuned using the lineshape of the 780 keV transition which displays predominantly a shifted part. The best results were obtained under the assumption that the ^{212}Po nuclei recoil in the forward direction within a cone with an opening angle of $\pm 35^\circ$. The electron stopping power for ^{212}Po ions in Pb was interpolated using the semi-empirical tables of Northcliffe and Schilling [33] and corrected to take into account atomic structure effects [34, 35]. The nuclear stopping power, which is due to the interaction with the atoms of the medium as a whole, was taken into account according to the LSS theory [36] and the parameterization of the universal scattering function for a Thomas-Fermi potential given in Ref. [37]. To correct for the effect of microchanneling in the stopping medium, the nuclear stopping power was reduced by a factor $f_n = 0.7$ (cf. Refs. [35, 38] for more details). According to the calculation, the distribution of the stopping times of the ^{212}Po recoils is characterized by a mean value of 1.35 ps and a variance of about 0.37^2 ps^2.

The line-shapes of the transitions to be analyzed were obtained using the coincidence matrices by setting gates on fully stopped γ-ray peaks belonging to transitions depopulating levels lying below the level of interest. The response functions of the cluster detectors in our experiment was characterized by small asymmetry towards lower energies which was taken into account too. Further, for the line-shape analysis, the natural time-dependent functional form of the population $n_i(t)$ of the investigated level was used, namely,

$$n_i(t) = \sum_{k \geq i} C_{ik} exp(-\lambda_k t) \qquad (2)$$

which represents a superposition of exponentials with coefficients C_{ik} determined by the decay constants λ_k of the levels participating in the cascade and by the branching ratios at every level. In the general case, a fitting procedure which aims to determine simultaneously many decay constants is hindered by the necessity to find a multiparameter solution, including some parameters describing the non-observed or side-feeding. In the present case, however, it was established for all levels depopulated by Doppler-shifted transitions that their observed discrete feeding is slow, and responsible only for part of the intensity of the unshifted fraction of the line-shape. The rest of the feeding is very fast, corresponding to (nearly) direct population of the levels of interest. This feature significantly simplifies the analysis, since the intensity balance at every level unambiguously fixes the areas of the "slow" and "fast" fractions of the lineshape. Then, the only remaining parameter to be determined is the decay constant of the level of interest or its lifetime ($\tau = 1/\lambda$).

Examples of line-shape analysis at the forward angle of 35° and the backward angle of 148° are displayed in figure 8, and all the results are summarized in tables VI and VII. As discussed previously (see sect. III B), most of these transitions have an E1 multipolarity. All

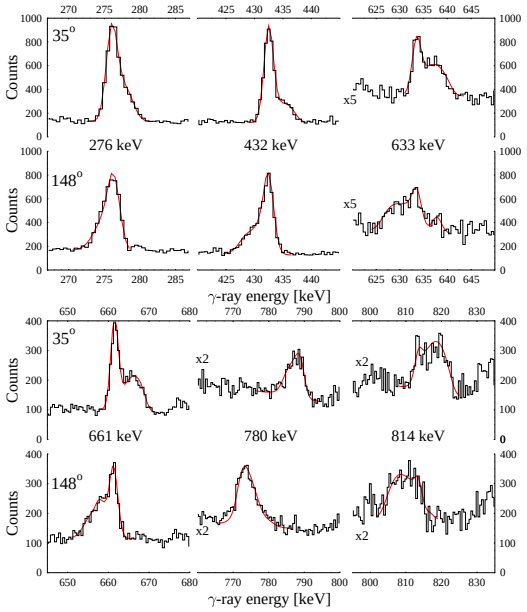

FIG. 8: (color online) Examples of line-shape analysis at the forward angle of 35° and the backward angle of 148°.

TABLE VI: Lifetimes measured in the present work with their uncertainties. The decomposition of the feeding intensity into slow and fast fractions is also indicated.

State (keV)	Feeding[a] Slow[%]	Fast[%]	Decay E_γ(keV)	$\tau^{(a)}$ (ps)
1744	33(7)	67(7)	612.3	0.48(15)
1751	68(4)	32(4)	276.1	0.48(20)
1787	68(3)	32(2)	432.3	0.45(8)
1946	13(4)	87(4)	813.6	0.47(15)
2016	44(3)	56(3)	661.3	0.49(16)
2465	30(4)	70(4)	633.3	0.61(16)
3155	≈ 0	≈100	780.4	0.12(6)

[a] the number in parenthesis is the error in the last digit.

TABLE VII: Limit values of the lifetimes derived in the present work.

State (keV)	Decay E_γ(keV)	$\tau^{(a)}$ (ps)	State (keV)	Decay E_γ(keV)	$\tau^{(a)}$ (ps)
2667	563.8	$\leq$ 1.4	2975	1620	$\leq$ 1.4
2837	1005	$\leq$ 1.4	3011	406.6	$\leq$ 1.4
2860	757.2	$\leq$ 1.4	3024	1669	$\leq$ 1.4
2864	490.2	$\leq$ 0.55	3203	1371	$\leq$ 1.4
2867	397.7	$\leq$ 1.4	3210	740.2	$\leq$ 1.4
2881	1049	$\leq$ 0.55			

the other transitions having an energy lower than 1 MeV are also assigned as E1, since their transition strengths, calculated for M1 or E2 multipolarities, would lead to unexpectedly large values.

The values of the B(E1) reduced transition probabilities have been calculated, taking into account the experimental values of the α_{tot} coefficients (see table V). The results, given in table VIII, are displayed, as a function of their location in the level scheme, in fig. 9 and will be discussed in Sect. IV D.

TABLE VIII: Values of the B(E1) reduced transition probabilities of the enhanced E1 γ-rays measured in this work.

E_γ(E1) (keV)	B(E1)[a] (e^2fm^2)	B(E1)[a] (W.u.)
276.1	4.6(23) 10^{-2}	2.0(10) 10^{-2}
398.0	$\geq$ 7.0 10^{-3}	$\geq$ 3.0 10^{-3}
406.6	$\geq$ 6.5 10^{-3}	$\geq$ 2.8 10^{-3}
432.3	1.5(3) 10^{-2}	6.6(12) 10^{-3}
490.2	$\geq$ 9.6 10^{-3}	$\geq$ 4.2 10^{-3}
563.8	$\geq$ 1.7 10^{-3}	$\geq$ 7.6 10^{-4}
612.3	5.7(18) 10^{-3}	2.5(7) 10^{-3}
633.3	4.1(11) 10^{-3}	1.8(5) 10^{-3}
661.3	4.4(14) 10^{-3}	1.9(6) 10^{-3}
740.2	$\geq$ 1.1 10^{-3}	$\geq$ 4.8 10^{-4}
757.2	$\geq$ 1.0 10^{-3}	$\geq$ 4.5 10^{-4}
780.4	1.1(6) 10^{-2}	4.8(26) 10^{-3}
813.6	2.5(8) 10^{-3}	1.1(3) 10^{-3}

[a] the number in parenthesis is the error in the last digit.

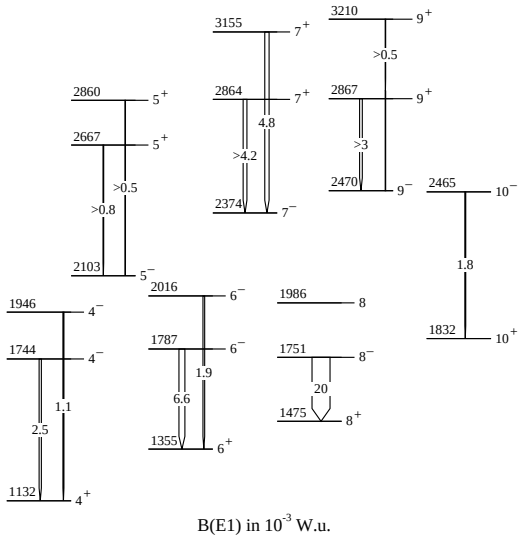

FIG. 9: States of ^{212}Po decaying by enhanced E1 transitions, the width of each arrow is proportional to the B(E1) value (given in 10^{-3} W.u.).

E. Peculiarity of the ^{212}Po level scheme obtained in this work

A close examination of fig. 6 reveals that the same basic structure arises three times, which expands above

the I^+ yrast states with I = 4, 6, 8 (the fact that this was not observed above the 2_1^+ state in our experiment can be due to the trigger level used to record the events). This structure comprises:

- two I^- states (drawn in magenta) which only decay to the I^+ yrast state *via* an enhanced E1 transition.
- one $(I + 1)^-$ (drawn in blue) which decays to the I^+ and $(I + 2)^+$ yrast states, as well as to the two I^- states (drawn in magenta). Moreover, in two cases, the decay to the low-lying $(I + 2)^-$ state is also observed.
- two $(I + 1)^+$ states (drawn in violet) which only decay to the $(I + 1)^-$ states (drawn in blue) *via* an enhanced E1 transition.

Such a feature gives confidence in the spin and parity assignments we have done using all the experimental results reported in the previous sections.

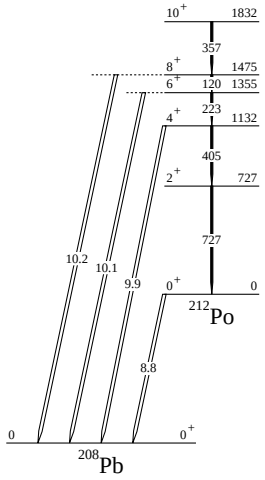

FIG. 10: Schematic representation of the α decay-lines of ^{212}Po [43]. Values of α energies are given in MeV, whereas those of γ-transition and level energies of ^{212}Po are given in keV.

F. α branching ratios

Several yrast states of ^{212}Po were reported to partially decay *via* α emission to the ground state of ^{208}Pb, as the corresponding α lines were clearly identified [39–42]. The branching ratios given in column 4 of table IX are those quoted in the last evaluation of the nuclear spectroscopic information for the A=212 nuclides [43]. It is noteworthy that the numbers for the 4^+, 6^+, and 8^+ states are very large, they come from the analysis of the β decay of the 9^- isomeric state of ^{212}Bi which populates excited states of ^{212}Po (see ref. [42]). The value, $b_\alpha(8^+)\sim 42\%$, is well greater than the one previously determined using α-γ coincidence [40], $b_\alpha(8^+)\sim 6\%$.

TABLE IX: α branching ratios (b_α) of the first yrast states of ^{212}Po given in the last evaluation of the nuclear spectroscopic information for the A=212 nuclides [43]. The new values are evaluated from refs. [39–41] as well as our results (see text). The new values of $T^\alpha_{1/2}$ are given in the last column.

State (keV)	I^π	$T_{1/2}$ ns	b_α (%) from [43]	b_α (%) new value	$T^\alpha_{1/2}$ ns
0	0^+	299(2)	100	100	299(2)
727	2^+		0.033	0.033	
1132	4^+		~ 27	~ 0.5	
1355	6^+	0.76(21)	~ 71	$\sim 3(1)$	25(10)
1475	8^+	14.7(3)	~ 42	$\sim 3(1)$	490(150)

Large values of α branching ratios could easily be confirmed by intensity balances in our γ-spectra gated by at least one transition lying in the top of the level scheme. Indeed any α emission would lead to a loss of the total intensity (*i.e.* including electron conversion) of the transitions located below the α emitting state. From the analysis of such double-gated spectra, we did not confirm any large value of b_α: the five yrast transitions (357 keV, 120 keV, 223 keV, 405 keV and 727 keV) exhibit total intensities which are constant within the error bars.

In order to go further, we have carefully examined the four papers published on this subject [39–42]. Baidsen *et al.* [39] measured three α-lines of energies E_α = 9.89 MeV, 10.10 MeV, and 10.22 MeV (see fig. 10), having *relative* intensities of 8%, 46%, and 46%, respectively. These α lines were interpreted as the α-decays of three excited states of ^{212}Po, lying above 1 MeV excitation energy. Simultaneously, from results of $\alpha - \gamma$ coincidences and half-life measurements, Lieder *et al.* [40] established (i) a 10.18 MeV α line deexciting a state with $T_{1/2}$=14.2(24) ns in ^{212}Po and (ii) several γ transitions correlated in time with the 8.78 MeV α line emitted by the ground state of ^{212}Po. This led to the identification of the 4^+, 6^+ yrast states (from the cascade 223-405-727) and the 14.2 ns isomeric state was interpreted as the 8^+ yrast state, at 1423 ± 30 keV from the energy balance of the α and γ lines. Moreover, the intensities of the α and γ transitions deexciting this new 8^+ state were found to be I_α=0.06(1) and I_γ=0.94(1), respectively.

This has been confirmed two years later from $\alpha - \gamma$ coincidences [41], particularly the 120 keV transition deexciting the 8^+ yrast state was measured for the first time and the α transition deexciting the 8^+ yrast state was clearly resolved from the one deexciting the 6^+ yrast state, both with similar intensity, whereas the line associated with the 4^+ state was well weaker (in agreement with results of ref. [39], above-mentioned).

At this stage, we can conclude that the 10.18 MeV α line of ref. [40] is the doublet (see fig. 10) of the two lines at 10.1 MeV and 10.2 MeV given in refs. [39, 41]. Thus the I_α value attributed at that time to the 8^+ yrast state (6%) has to be divided by 2, the second part being

ascribed to the α decay of the 6^+ yrast state. These results, which are quoted in column 5 of table IX, are now in quantitative agreement with our intensity balances.

The result of the β decay of the 9^- isomeric state of ^{212}Bi made by Eskola *et al.* [42], which was adopted in the last compilation [43], indicates very strong components of α emission from the yrast states of ^{212}Po which were neither found in the previous experiment [40] nor in our data set. Moreover, the α spectrum displayed in that paper does not corroborate such a result, as the intensity of the α group of ~ 10 MeV is less than the one corresponding to the ^{212}Po ground state decay, by more than one order of magnitude. So we can wonder whether there is a misprint in ref. [42], the number of α decay of the excited states being reversed with the one of the ground state.

The new values of the α partial half-lives of the yrast states are given in the last column of table IX, they will be discussed in the next section in connection with the cluster structure of the states.

IV. DISCUSSION

It would be very straigthforward to predict the structure of ^{212}Po, with four nucleons outside ^{208}Pb, in terms of shell-model (SM) configurations, using the single-particle states in the mean field of the doubly-magic core. Nevertheless as the four nucleons are two protons and two neutrons, we have also to take into account the four-particle correlation leading to the formation of the α-particle. In this section, we aim to isolate the effects of four-particle correlations on the properties of the excited states of ^{212}Po (excitation energy, spin and parity, de-excitation modes). For that purpose, we use *empirical* arguments from the comparison with the neighbouring isotopes and isotones which are mainly described within SM configurations.

Figure 11 displays most of the ^{212}Po states observed in the present work, grouped as a function of their underlying structures which are reviewed by turns:

- the yrast positive-parity states (in black) are discussed in terms of two-particle excitation, as their excitation energy as a function of angular momentum follows the typical curve expected in case of pair breaking [44]. Nevertheless several features point out the simultaneous effect of four-particle correlations (sects. IV A and IV B)

- the negative-parity states (in blue) involve the coupling of the low-lying 3^- octupole vibration to the excitation of the valence neutrons (sect. IV C)

- the non-natural parity states (in magenta, orange, and violet) are the fingerprints of the 'α + ^{208}Pb' structure (sect. IV D).

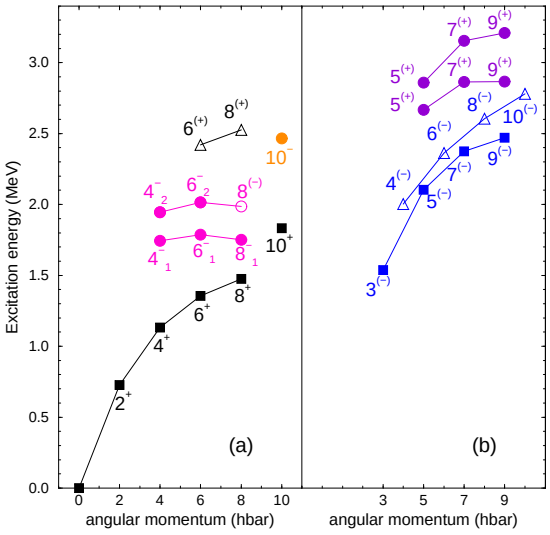

FIG. 11: (color online) Excitation energy as a function of angular momentum of most of the ^{212}Po states observed in the present work (they are displayed in figs. 5 and 6 using the same colors). Each state drawn with a filled circle (magenta, orange, and violet) decays by an enhanced E1 transition towards the state with the same angular momentum.

A. Is the nucleon-pair breaking the unique excitation mode of ^{212}Po at low energy?

The first excited states of ^{210}Pb$_{128}$ and $^{210}_{84}$Po are text-book examples of residual interaction in a two-particle configuration, namely $(\nu g_{9/2})^2$ and $(\pi h_{9/2})^2$, respectively. While the energy interval of the whole multiplet extends over 1557 keV for the two-proton case, the one of the two-neutron configuration is more compressed (1278 keV) (see the top part of fig. 12). That is directly connected to the energies of the residual interactions, as discussed below.

The structure of the first levels of $^{212}_{84}$Po$_{128}$ (see fig. 12) would be described as a superposition of the excitations known in its two even-even neighbours. The low energy of the 2^+_1 state (727 keV) indicates that the $(\nu g_{9/2})^2$ part of its wave function is likely stronger than the $(\pi h_{9/2})^2$ one. The fact that the neutron pair breaks more easily than the proton one beyond the doubly-magic nucleus ^{208}Pb, is corroborated by the empirical values of the proton (neutron) pairing energies extracted from the measured binding energies of the ground states of the odd-Z (odd-N) nuclei surrounding ^{212}Po. In order to avoid the effect of the extra binding energy of the doubly-magic nucleus ^{208}Pb, we use the three-point formula [45], defining a local average of the masses of two odd-A nuclei which is compared with the observed mass of the even-even ^{212}Po nucleus:

$$\Delta_p^{(3)}(84) = BE(84,128) - \frac{1}{2}\left[BE(83,128) + BE(85,128)\right] \quad (3)$$

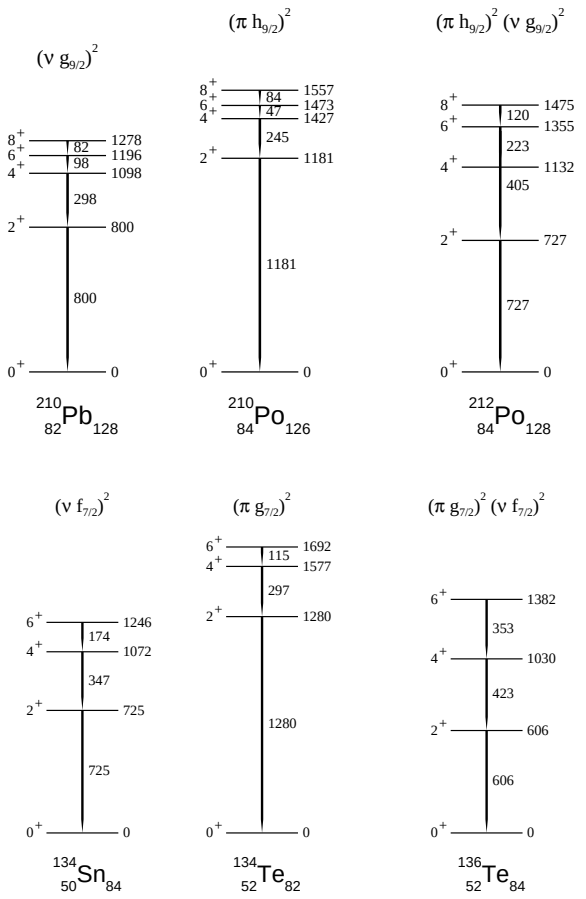

FIG. 12: **Top**: First excited states of ^{210}Pb, ^{210}Po, and ^{212}Po, the three 8^+ levels are isomeric ($T_{1/2}$ = 201(17) ns, 98.9(25) ns, and 17.1(2) ns, respectively). **Bottom**: First excited states of ^{134}Sn, ^{134}Te, and ^{136}Te. The 6^+ levels of ^{134}Sn and ^{134}Te are isomeric ($T_{1/2}$ = 80(15) ns and 164.1(9) ns, respectively).

$$\Delta_n^{(3)}(128) = BE(84,128) - \frac{1}{2}\left[BE(84,127) + BE(84,129)\right] \quad (4)$$

The neutron pairing energy, $\Delta_n^{(3)}$= 826(2) keV, is lower than the proton one, $\Delta_p^{(3)}$= 1150(3) keV, by $\sim$ 320 keV[3].

Noteworthy is the fact that a similar situation occurs in other nuclei located just above the doubly-magic core of ^{132}Sn (see the bottom part of fig. 12). Firstly, the two-neutron configuration of ^{134}Sn leads to a more compressed level scheme than the two-proton configuration of ^{134}Te. Secondly, the low energy of the 2_1^+ state of ^{136}Te occurs in concert with a low value of the neutron pairing energy. The three-point formula give $\Delta_p^{(3)}(52)$ = 1320(60) keV and $\Delta_n^{(3)}(84)$ = 730(82) keV. Thus the neutron pair breaks more easily than the proton one and the 2_1^+ wave function of ^{136}Te should contain a large component of neutron excitation. Such a scenario is strengthened by the B(E2; $0^+ \rightarrow 2_1^+$) values, which have been recently measured by Coulomb excitation in inverse kinematics [46]. The value obtained in ^{134}Te (4.7(6) W. u.) is stronger than the ^{134}Sn one (1.4(2) W. u.), as expected from their different excitation processes (breaking of a proton pair versus a neutron pair). Moreover the result obtained in ^{136}Te has confirmed that the wave function of its 2_1^+ state mainly comes from neutron excitation [47, 48].

Unfortunately the leading role of neutron excitation in the wave function of the 2_1^+ state of ^{212}Po cannot be validated by the value of the B(E2) reduced transition, as it is not known. Nevertheless the comparison of the B(E2) values within the seniority-2 states of the three neighbours is especially instructive in this respect (see fig. 13). As expected, the values of ^{210}Po are larger than those of

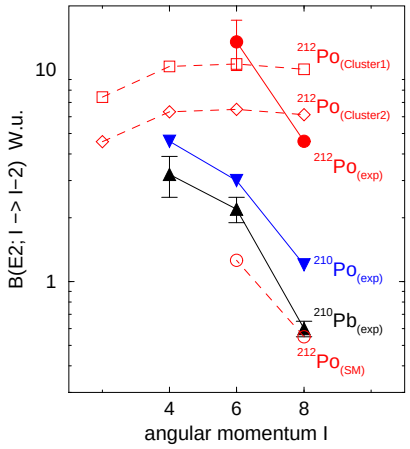

FIG. 13: (color online) Experimental values of the reduced transition probabilities B(E2; I $\rightarrow$ I-2) of the first yrast states of $^{210}_{82}$Pb$_{128}$ (ref. [28]), $^{210}_{84}$Po$_{126}$ (ref. [28]), and $^{212}_{84}$Po$_{128}$ (ref. [4] and this work). The theoretical values of ^{212}Po come from shell-model approach [4], and from α-^{208}Pb cluster models (Cluster1 from ref. [10], Cluster2 from ref. [12]).

^{210}Pb, owing to their different excitation processes (proton pair *versus* neutron pair). Similarly the values of the 6_1^+ state and 8_1^+ state of ^{212}Po, calculated using the shell-model approach [4] (see the empty circles in fig. 13) are low since these states are predicted to come mainly from neutron excitation, as above-mentioned. On the other hand, the measured values (ref. [28] and this work for the new values of the α / γ branching ratios) are greater than the calculated ones by one order of magnitude, implying that these 6_1^+ and 8_1^+ states are complex. Even though their energies are rather well reproduced from the sole two-neutron excitation, other excitation modes have to be taken into account, such as the α + ^{208}Pb cluster states which lead to very large values of B(E2) as displayed in fig. 13.

[3] The same difference is obtained when computing $\Delta_p^{(3)}(84)$ associated to ^{210}Po and $\Delta_n^{(3)}(128)$ associated to ^{210}Pb.

Before closing this section, we want to recall what SM configurations were attributed to the high-spin yrast states [4]. The excitation of one neutron to the second orbit above the magic number gives the $\nu g_{9/2}\nu i_{11/2}$ configuration, whereas the excitation of one nucleon to the first intruder orbit above the magic numbers gives either $\nu i_{11/2}\nu j_{15/2}$ or $\pi h_{9/2}\pi i_{13/2}$. Thus, we expect three multiplets of states with spin values $I^\pi = 1^+$ to 10^+, 2^- to 13^-, and 2^- to 11^- respectively. Since the two nucleons have the same character (particle-particle), the energies of the states having the extreme spin values (1^+ and 10^+, 2^- and 13^-, and 2^- and 11^- respectively) are the most lowered by the residual interactions. That provides reliable assignments for the yrast states located at 1832 keV (10^+), 2769 keV (13^-), and 2409 keV (11^-). It is worth pointing out that in the framework of the SM approach, the levels with $I^\pi = 4^-$ to 9^- are expected above 2409 keV, the energy of the lowest negative-parity level. As for the higher spin values ($I > 10^+$), they are obtained from the simultaneous excitation of the two pairs of nucleons, $(\nu g_{9/2})^2 \otimes (\pi h_{9/2})^2$ ($I_{max} = 16^+$) or $(\nu g_{9/2}\nu i_{11/2}) \otimes (\pi h_{9/2})^2$ ($I_{max} = 18^+$).

B. Are the α-decays of ^{212}Po enhanced ?

Besides its ground state which decays by α emission, ^{212}Po has several excited states which are also α emitters, some of the partial half-lives are given in the last column of table IX (sect. III F). The present section is devoted to the comparison of the α-emission probabilities of ^{212}Po to those of the neighbouring isotopes and isotones in order to show *empirically* that the cluster structure, $\alpha + {}^{208}$Pb, plays an important role in the process.

The well-known Geiger-Nuttall plots show the correlation between the decay half-life and the energy of the emitted α:

$$log_{10}T_{1/2} = aE_\alpha^{-1/2} + b \qquad (5)$$

The parameters are usually obtained by fitting the data associated to the ground states of nuclei of each isotopic series. It is important to note that when an isotopic series crosses a neutron magic number, such as N=126, the results separate into two groups, each one having its own parameters [49]. In parallel, intensive works have been done in order to obtain a *universal* description of α decays, as well as cluster radioactivity (see, for instance, the new law recently published in ref. [50]).

For our purpose, we have only used the data associated to nuclei with N=130-136 of four isotopic series ($_{84}$Po, $_{86}$Rn, $_{88}$Ra, $_{90}$Th), excluding the nuclei of interest, the N=128 isotones. The values of the two coefficients of the Geiger-Nuttall relations (eq. 5) are given in table X and the fits are drawn in fig. 14. The half-life values extend over 10 orders of magnitude, thus we give a zoom on the behaviour of the four N=128 isotones, in the inset of fig. 14. Their measured α half-lives are greater than the values expected from the fits (each empty symbol lies above the corresponding line), allowing us to calculate the hindrance factors (HF), i.e. the ratio of the experimental half-life and the extrapolated value (given in the last column of table X). Equation (5) mainly accounts for the α tunnelling through the potential barrier, but does not take into account any variation of the probability of α formation in the parent nuclei. Actually the quality of the fits shown in fig. 14 proves that this probability remains almost the same along an isotopic series as soon as *at least* two pairs of neutrons are available (i.e. N$\geq$ 130). On the other hand, the hindrance factors of the N = 128 isotones (HF > 1) mean that it is more difficult to form an α particle in the parent nuclei which have *only* two neutrons above a magic number. As seen in the last column of table X, the HF values increase regularly as Z is decreasing from $Z = 90$ to 86, while the value for $^{212}_{84}$Po is almost the same as the $^{214}_{86}$Rn one. This means that the ^{212}Po half-life is smaller than expected from the behaviour of its heavier isotones. Such a result is likely due to a greater value of the probability of α formation in the

TABLE X: Values of the two coefficients of the Geiger-Nuttall relations (eq. 5) describing the α-decay half-lives of the ground states of nuclei having N $\geq$ 130. The last column gives the value of the hindrance factor (HF) of each N=128 isotone (see text).

	N	a	b	HF(N=128)
$_{90}$Th	130-136	139.4±1.4	-51.98±0.50	1.4
$_{88}$Ra	130-136	136.1±0.9	-51.50±0.35	1.8
$_{86}$Rn	130-136	131.9±1.5	-50.84±0.58	2.2
$_{84}$Po	130-134	128.8±0.4	-50.30±0.16	2.3

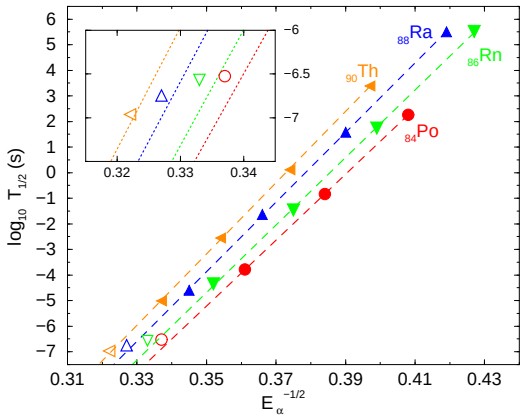

FIG. 14: (color online) Geiger-Nuttall relations for four sets of isotopes ($_{84}$Po, $_{86}$Rn, $_{88}$Ra, $_{90}$Th) having N=130-136 (filled symbols). The experimental data for$N$=128 are drawn with empty symbols. The inset gives a zoom on the four fits to emphasize the behaviour of the N=128 isotones, ^{218}Th (triangle left), ^{216}Ra (triangle up), ^{214}Rn (triangle down) and ^{212}Po (circle).

^{212}Po ground state, a sign of its cluster structure, α + ^{208}Pb. It is worth recalling that the amount of clustering predicted by an hybrid model comprising both shell and cluster configurations [8] is high (30%).

Using the partial half-lives given the last column of table IX, the HF values of two excited states of ^{212}Po can be computed as well, HF(6_1^+) = 1.8×10^2 and HF(8_1^+) = 6.0×10^3. In those cases, because of the conservation of the total angular momentum, the alpha emission occurs at non-zero value of orbital angular momentum, giving rise to a centrifugal potential which increases the potential barrier and slows down the tunnelling process [51]. It would have been interesting to make quantitative comparisons with transitions involving similar variations of angular momentum in neighbouring nuclei, in order to look for hint of cluster structure in these excited states. Unfortunately the number of cases available in the literature [28] is too scarce.

Finally we have to note that the new values of the α branching ratios of the 4_1^+, 6_1^+ and 8_1^+ states given in table IX are in good agreement with the predictions of the α-cluster models of ^{212}Po (see for instance refs. [10, 12]).

C. Excitations due to an octupole mode in ^{212}Po

The octupole mode is well known in the heavy nuclei. It gives rise to the lowest excited state of ^{208}Pb, with E = 2.614 MeV and $I^\pi = 3^-$, the E3 transition towards the ground state being collective, B(E3) = 33.8(6) *W.u.*. The structure of this octupole vibration comprises many coherent particle-hole excitations across the two magic gaps at $Z = 82$ and $N = 126$ involving several single-particle orbits with $\Delta l = 3$. When the Fermi levels are located well above these two gaps, namely for $N \sim 134$ and $Z \sim 88$, the octupole mode is enhanced because of strong octupole couplings between two pairs of orbits ($\nu g_{9/2} - \nu j_{15/2}$ in the one hand, $\pi f_{7/2} - \pi i_{13/2}$ in the other hand).

In between, there are various mixings of the 3^- excitation of the ^{208}Pb core and the single-particle excitations from these pairs of orbits. For instance, in ^{210}Pb, the 3^- collective excitation of the core and the 3^- state of the $\nu g_{9/2} - \nu j_{15/2}$ configuration, expected close in energy, are so strongly mixed that the measured octupole strength is split into two states 1 MeV apart (1869 keV and 2828 keV). They account for the full B(E3) intensity which has been observed in ^{208}Pb and as they share this intensity in the ratio 2:1 [52], the energy of the 3^- collective excitation can be computed, E $\sim$ 2.2 MeV.

Moreover, one can expect that adding nucleon pairs to ^{208}Pb would result in a greater softness of the collective 3^- octupole mode, with a lowering of its energy well below 2.614 MeV. This was put forward in order to explain the behaviour of the E3 strength in the $N = 127$ isotones, in the framework of particle-octupole vibration coupling [53]. The evolution of the excitation energy of the 3^- collective state is displayed in fig. 15, both as a function of Z and as a function of N. The decrease in energy is linear when adding proton pairs or neutron pairs to the doubly-magic core. The slope is $\sim$ 220 keV per proton pair (see the blue solid line in fig. 15a) and $\sim$ 400 keV per neutron pair (see the blue dotted line in fig. 15b). On the other hand, the decrease is stronger when adding both proton pairs and neutron pairs (see the slopes of the red or green lines).

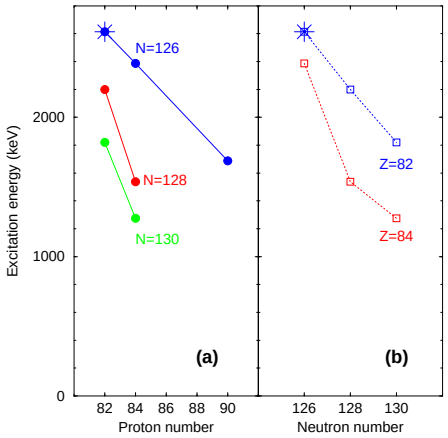

FIG. 15: (color online) Evolution of the excitation energy of the 3^- collective excitation when adding nucleon pairs to the ^{208}Pb doubly-magic core (marked with a star), as a function of the proton number (a) and of the neutron number (b).

The case of ^{212}Po seems peculiar as shown by the break in the red dotted line (see fig. 15b). When assuming a linear behaviour as a function of neutron number for $Z = 84$, the energy of its 3^- state would be 300 keV higher than measured. This is more likely the result of some mixing. It could involve the $\nu g_{9/2} - \nu j_{15/2}$ configuration as in ^{210}Pb, discussed above. Nevertheless the effect of the cluster structure, α + ^{208}Pb, should not be neglected. It is worth pointing out that the 10.302 MeV α-ray, observed in ref. [41], that defines an excited state at 1547(10) keV [28] could be assigned to the 3^- state at 1537 keV. The fact that the α-emission can compete with the γ decay would be a sign of a cluster part in the wave function of the 3^- state.

At higher excitation energy, we can expect negative-parity states from the coupling of the 3^- collective state to the valence nucleon excitation. In principle, several multiplets of states should be grouped at excitation energies given by the 3^- energy and the positive-parity yrast spectrum. Because of the residual interactions, the multiplets are no longer degenerated in energy and the highest-spin states of each multiplet would be the lowest ones. Such a behaviour is well known in the region of ^{146}Gd, where the octupole excitation also plays an important role.

The yrast states of ^{148}Gd with two valence neutrons outside the ^{146}Gd core nucleus have been identified and discussed in terms of spherical shell model and couplings

of two valence nucleons to one octupole phonon [54]. The four lowest yrast states up to 6^+ arise from the $\nu f^2_{7/2}$ configuration (see the left part of fig. 16). The coupling of this configuration to the ^{146}Gd 3^- core phonon gives rise to a lot of negative parity levels. Some of them are mixed with the states from the excited $\nu f^1_{7/2}\nu i^1_{13/2}$ configuration which gives a multiplet of eight states ($3^- \leq I^\pi \leq 10^-$). As a result, the first states with negative-parity display a characteristic behaviour, one branch is formed by the first states having the odd values of angular momentum, while the first states having the even values are located slightly higher in energy (see the blue symbols in the left part of fig. 16). Lifetimes of excited states in ^{148}Gd were measured [55]: all the B(E1) values of the transitions linking the negative-parity states with odd spin values to the positive-parity yrast states are around 10^{-5}-10^{-6} W.u., i.e. within the "normal" range.

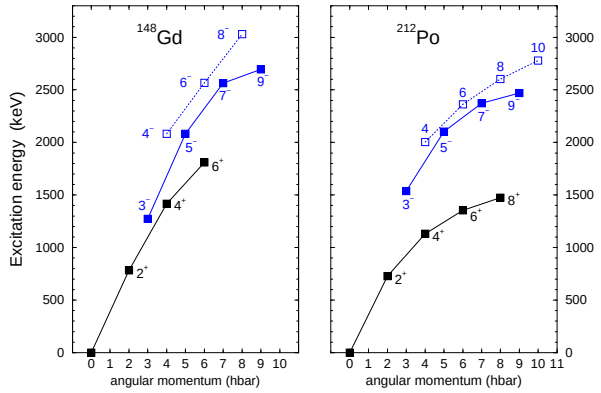

FIG. 16: (color online) Left: Excitation energy, as a function of angular momentum, of some states of $^{148}_{64}Gd_{84}$, which can be interpreted in terms of spherical shell-model configurations (black symbols) and couplings of two valence nucleons to one octupole phonon (blue symbols), from ref. [54]. Right: Similar states of $^{212}_{84}Po_{128}$ observed in our experiment.

It is worth pointing out that the two neutron shells involved in ^{148}Gd have their counterparts in ^{212}Po, with one unit larger angular momenta l and j ($\nu f_{7/2} \rightarrow \nu h_{9/2}$ and $\nu i_{13/2} \rightarrow \nu j_{15/2}$). This allows us to make reliable extrapolations to the case of ^{212}Po. The comparison between the left and the right parts of fig. 16 indicates unambiguously that the branch comprising the 5^-, 7^-, and 9^- states comes mainly from the couplings of two valence nucleons to one octupole phonon. Moreover, four states with even-spin values (at 2003, 2363, 2604, and 2780 keV), which decays the odd-I states, probably form the second branch of negative-parity states in ^{212}Po as observed in ^{148}Gd (see the blue open squares in fig. 16).

D. Cluster structure of the low-lying states of ^{212}Po

Many theoretical works were devoted to the calculations of low-lying states of ^{212}Po assuming an *unmixed* α-^{208}Pb cluster structure (see for instance refs. [9–12]), the potential being either phenomenological with different forms (such as square well, cosh potential, or a modified Woods-Saxon function), or obtained from a double folding procedure (i.e. the real part of the optical potential giving a good description of the α + ^{208}Pb scattering). In both cases, the numerical values of some free parameters were determined to reproduce the energies of the yrast states of ^{212}Po, either exactly [9–11] or at the best [12]. It is worth pointing out that without these free parameters, all the predicted spectra of the yrast states are inverted (the highest-spin states lying below the lowest-spin ones, at variance with the experimental data). The main success of these calculations (as mentioned above, at the end of sect. IV A and fig. 13) is the better description of the B(E2) values inside the ground-state band, indicating that the wave-function of the yrast states having even-I and positive-parity values do possess some cluster content.

1. *Enhanced E1 transitions*

A major result of the present work is the observation of many strongly enhanced E1 transitions connecting several excited states to the yrast ones, having the same spin values (see fig. 9). Moreover as outlined above (at the end of sect. IV A), non-natural parity states, such as 4^-, 6^-, and 8^-, are not expected below 2.4 MeV excitation energy in the SM approach.

Enhanced B(E1) values are commonly found in nuclei exhibiting an *electric dipole moment*, such as light nuclei described in terms of a bimolecular system rotating about its center of mass, or heavy nuclei displaying octupole deformation [56, 57]. Some typical values are shown in fig. 17 using filled symbols (Sm isotopes with $N \sim 90$, ^{225}Ra and ^{225}Ac [28], cluster states of ^{18}O [58]). They are one order of magnitude greater than those of transitions measured in octupole-vibrational nuclei, such as ^{148}Gd, ^{225}Ac, ^{231}Th, ^{231}Pa (shown with empty symbols) and three orders of magnitude greater than those of single-particle transitions in Bi isotopes.

More generally, when a nucleus clusterizes into fragments with different charge to mass ratios, the center of mass does not coincide any more with the center of charge, and a sizeable static E1 moment may arise in the intrinsic frame [59]. The dipole moment is

$$D = e(Z_1 + Z_2)[\frac{Z_2}{(Z_1 + Z_2)} - \frac{A_2}{(A_1 + A_2)}] \times q \qquad (6)$$

where the parameter q is the distance between the centers of mass of the two fragments (see Eq. (1) of Ref. [59]). Assuming two spheres in contact, the dipole moment of

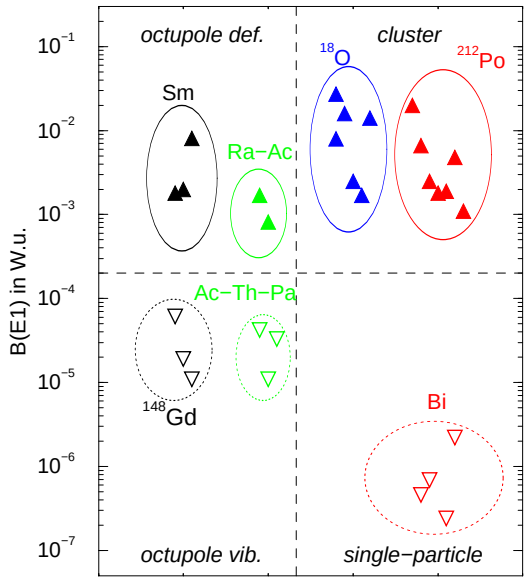

FIG. 17: (color online) Values of B(E1) transition rates (in Weisskopf units) for typical cases: Transitions in octupole-deformed and octupole-vibrational nuclei, transitions between single-particle states, and transitions involving cluster states.

the α+^{14}C system is 0.9 $e$fm and very large values of E1 rates have been found in ^{18}O [58] (see the blue symbols in fig. 17). In the same way, the value of the α+^{208}Pb system is as large as 3.7 $e$fm, which would lead to very enhanced E1 transitions. It is worth noting that the E1 rates measured in the present work (shown with the red filled symbols in fig. 17) are definitely located in the top part of the figure. This shows the 'α+^{208}Pb' structure of the even-I negative-parity states, which can be considered as *pure* cluster states since they are too low in energy to be accounted for using the SM approach (see the end of sect. IV A).

One way of characterizing the cluster content of states, which has been commonly done for the light nuclei, is measuring their α-decay width. Because of their non-naturalα parity, the α-decay of the ^{212}Po cluster states to the ^{208}Pb ground state is expected to be forbidden (parity violation), although the energy factor would be very favourable. On the other hand, the α-decay of the ^{212}Po cluster states to the 3^-_1 excited state of ^{208}Pb is allowed. Nevertheless the available energy for such an α emission is so low that the α-decay cannot compete with the very enhanced γ-decays, measured in the present work.

2. *A possible model*

Following the ansatz of Ref. [8] dealing with the ground state of ^{212}Po and taking into account the conclusions of the previous sub-sections, we suppose that the wave function of *every* excited state of ^{212}Po can be written as the sum of two parts:

$$\Psi^{tot}(I^\pi) = a\ \Psi^{SM}(I^\pi) + b\ \Psi^{cluster}(I^\pi) \qquad (7)$$

where Ψ^{SM} stands for the pure shell-model piece and $\Psi^{cluster}$ takes account of the α clustering. This is the same as in our previous work [13] with this difference that here we formulate the latter using a more microscopic point of view. It may be obtained from a GCM calculation in the following way,

$$\Psi^{cluster} = \int' dq f(q) |HFB(q)\rangle|_{N,Z}, \qquad (8)$$

where the indices N, Z indicate that the HFB wave function is projected on good particle number (neutrons and protons). The variable q indicates the very asymmetric fission path of the α particle on its way to disintegration. In the end of the process, q will correspond to the relative distance of the c.o.m. coordinates of the Pb core and the α particle. In fig. 18 we show a series of typical "Pb + α" shapes which $|HFB(q)\rangle$ should contain as a function of q (we agree that such shapes would be difficult to create technically: It is like a very asymmetric fission calculation).

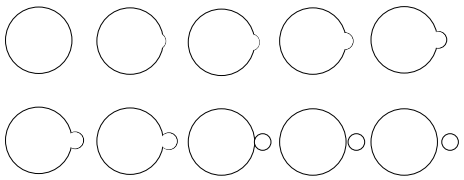

FIG. 18: Typical ^{208}Pb +α shapes as a function of the distance between their center of mass.

One should be aware of the fact that $|HFB(q)\rangle$ expressed in terms of excitations of the spherical ^{208}Pb core + valence particles contains complicated many particle-many hole configurations (many quasi-particle configurations) such as, e.g. 5p-1h, 6p-2h,...9p-5h, etc., creating the cluster configuration. We put a prime on the integration sign to indicate that we took out of the sum the 4p-0h shell-model configurations, Ψ^{SM}, which we wrote formally apart in eq. 7 in order to ease discussions below.

After minimisation of energy with respect to the amplitudes $f(q)$ the corresponding GCM Schroedinger equation will supposedly contain a typical double-well potential for the α particle sitting on the right or left hand side of the Pb core. We suppose that the individual potential wells are deep enough to accomodate two states, the ground state and an excited state (ν= 0 and 1). The excited state may be interpreted as a vibration of the α particle against the ^{208}Pb core. The finite barrier will allow for tunnelling and the left-right degeneracy will be lifted to give rise to *four* different states with alternating

parities,

$$\varphi^{\pm}_{0,1} = \frac{1}{\sqrt{2}}[\varphi^{R}_{0,1} \pm \varphi^{L}_{0,1}]. \quad (9)$$

The next step is to project the four wave functions on good spin value. We surmise that the small α-grain on top of ^{208}Pb perturbs sphericity only slightly. It will produce double-well scenarios weakly depending on spin. This naturally will produce for each spin quadruplets of states with alternating parities, i.e. four components $\Psi^{cluster}_{0,1}(I^{\pm})$ for eq. 7. Let us mention that spin projection also takes care of the $l = 1$ mode where the α particle vibrates against the Pb core.

These four cluster states still have to be mixed and orthogonalized with the SM configurations as indicated in eq. 7. Among the low-lying quadruplet of states belonging to the yrast band, only the positive-parity states will be affected. Actually the mixing may be relatively strong (it is predicted that the ground state contains about 30% alpha-cluster configuration [8]) pushing the other positive parity states up into energy regions where the highest member is yet to be detected. This also eventually explains why the natural order of +, -, +, - parities is changed to +, -, -, +. This picture qualitatively explains the experimental situation for the quadruplet of states of even spin comprising the ones of the yrast band (see fig. 11a). One easily imagines that the projection on odd-spin values creates states at higher energy, since already at sphericity the odd-spin, negative-parity states are above the ones with even spins. Therefore, the whole scenario shown in fig. 11 could find a natural explanation within the above lines of thought.

To be slightly more specific, let us discuss a completely phenomenological model imitating schematically the GCM calculation. The deformation Hamiltonian is then

$$H^{(I)}_{coll} = -\frac{\hbar^2}{2M}\frac{\partial^2}{\partial q^2} + V(q) \quad (10)$$

where M is an adjustable inertia, depending eventually on spin and $V(q)$ is a double-well potential which for convenience may be taken as a double-oscillator potential, a typical textbook example [60], which is sketched in the top part of fig. 19. The barrier penetration, which is a function of the q_0 value, leads to the energy splittings of the $\varphi^{\pm}_0$ and $\varphi^{\pm}_1$ eigenstates (cf. eq. 9): The relative energies of these four states are drawn in the bottom part of fig. 19.

The potential parameters also may depend on spin stemming from the spin projection. Using the dipole operator, as defined in eq. 6 and supposing that the cluster configuration of the even-parity yrast states is admixed with 30 percent, we get a right order of magnitude for the $B(E1)$ values. Making the oscillator length of the potential slightly spin dependent, we also can reproduce the falling tendency of B(E1) vs $\Delta E(I)$ (see fig. 9) rather accurately.

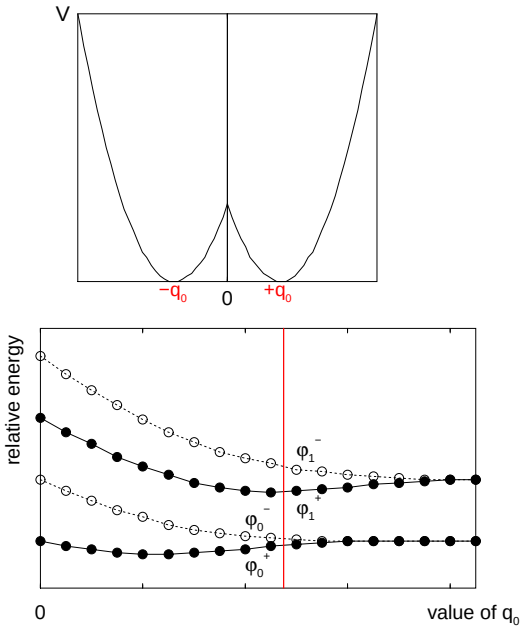

FIG. 19: **Top**: $V(q)$ for a double-oscillator potential. **Bottom**: Relative energies, versus the distance between the two minima, for the four lowest eigenstates of the double oscillator. When $q_0 = 0$, the eigenvalues are those of a simple harmonic oscillator. When the two wells are completely separated, (large value of q_0), the energies of $\varphi^{\pm}_0$ are degenerated, as well as those of $\varphi^{\pm}_1$. The vertical line indicates the four energies obtained for a typical value of q_0.

The above scenario remains on a very schematic level. It should be verified by more microscopic studies which are planned for the future.

3. Outlook

The oscillatory motion of the α-core distance around the equilibrium position is proposed for the first time. This would be a novel manifestation of α-clustering, never noticed in light systems. In those cases, the α-core system can rotate collectively about its center of mass (for a review of the so-called nuclear molecules, see [61]) and it is probably difficult to isolate an oscillatory motion, if any.

In the chart of nuclides, there are two cases similar to ^{212}Po: $^{104}_{52}$Te as 'α+^{100}Sn' and $^{136}_{52}$Te as 'α+^{132}Sn'. These α-core systems fulfill the two prerequisites:

- The ground state of the composite nucleus is above or close to the α-decay threshold (cf. the *Ikeda* diagram displayed in fig. 1 of ref. [61]).

- The center of mass of the α-core system is nearly merged with the center of the spherical core, so as the system cannot rotate collectively.

Having the same value of dipole moment as ^{212}Po, ^{136}Te should exhibit enhanced electric dipole transitions. On the other hand, the decay of the cluster states of ^{104}Te should be different since the E1 transitions are hindered as there is no shift between the center of charge and the center of charge, the two clusters having $N = Z$. Thus the α emission could compete for their decay.

One may speculate that adding more α's to the ^{208}Pb core, like, e.g. two α's to give ^{216}Rn, may exhibit similar physics. For example the two α's may move coherently as a ^{8}Be and then the present scenario may repeat itself partially, or the two α's may move independently and, then, more complex structures can be expected.

V. SUMMARY AND CONCLUSIONS

In summary, we have used the transfer of an α-particle induced by a heavy-ion beam at very low energy to populate excited states of ^{212}Po. The level scheme has been extended up to ~ 3.2 MeV excitation energy. The γ angular distributions and $\gamma - \gamma$ angular correlations have been analyzed in order to assign spin and parity values to many observed states. Several γ lines with $E_\gamma < 1$ MeV have been found to be strongly shifted and broadened by the Doppler effect, allowing for the measurements of the corresponding lifetimes by the DSAM method. The values, found in the range [0.1-0.6] ps, lead to very enhanced E1 transitions.

The excited states of ^{212}Po can be distributed among two groups:

- The first one comprises all the states having natural parity. They bear strong resemblance with those identified in the neighbouring isotopes and isotones and can be explained in terms of single-particle excitations dealing with the neutron and proton orbits lying close to the Fermi levels, as well as their coupling to the 3^- octupole vibration. Nevertheless more stringent analysis reveals that several properties (such as B(E2) transition probabilities or α-emission probabilities) are not accounted for by such an interpretation.

- The second one comprises many states having non-natural parity which are mainly grouped into 2 sets, a first one with even-I values around 2 MeV excitation energy and a second one with odd-I values around 3 MeV. These levels only decay to the yrast states having the same I value, by very enhanced E1 transitions (B(E1) $\sim 2\times10^{-2}$ – 1×10^{-3} W.u.). They are the fingerprints of the 'α+^{208}Pb' structure.

Such an 'α+core' structure is observed for the first time. It could be also identified in two other systems, $^{104}_{52}$Te as 'α+^{100}Sn' and $^{136}_{52}$Te as 'α+^{132}Sn'. While these two Te isotopes are located very far from the stability valley, they could be close at hand, thanks to the new worldwide facilities soon available.

Acknowledgement The Euroball project was a collaboration between France, the United Kingdom, Germany, Italy, Denmark and Sweden. A.A., P.P. and M.-G.P. are very indebted to their colleagues involved in the EB-02/17 experiment devoted to the fission fragments, in which the present data on ^{212}Po were recorded. They thank the crews of the Vivitron, as well as M.-A. Saettle for preparing the Pb target, P. Bednarczyk, J. Devin, J.-M. Gallone, P. Médina and D. Vintache for their help during the experiment. We thank Dr. M. Mirea, Dr. W. Nazarewicz, Dr. W. von Oertzen, Dr. N. Rowley, and Dr. T. Yamada for fruitful discussions. This work was partially supported by the collaboration agreement between the Bulgarian Academy of Sciences and CNRS under contract No 16946, and by contract IDEI-119 of the Romanian Ministry of Education and Research.

[1] E. Rutherford and A.B. Wood, Phil. Mag. **31**, 379 (1916).
[2] I. Perlman *et al.*, Phys. Rev. **127**, 917 (1962).
[3] H. Bohn *et al.*, Zeit. Phys. A**302**, 51 (1981).
[4] A.R. Poletti *et al.*, Nucl. Phys. **A473**, 595 (1987).
[5] M. Sugawara *et al.*, Nucl. Phys. **A443**, 461 (1985).
[6] Zs. Podolyák *et al.*, Nucl. Instr. Meth. Phys. Res. A **511**, 354 (2003).
[7] A.B. Garnsworthy *et al.*, J. Phys. G **31**, S1851 (2005).
[8] K. Varga, R.G. Lovas and R.J. Liotta, Phys. Rev. Lett. **69**, 37 (1992) and Nucl. Phys. **A550**, 421 (1992).
[9] B. Buck, A.C. Merchant, and S.M. Perez, Phys. Rev. Lett. **72**, 1326 (1994).
[10] F. Hoyler, P. Mohr and G. Staudt, Phys. Rev. **C50**, 2631 (1994).
[11] S. Ohkubo, Phys. Rev. Lett. **74**, 2176 (1995).
[12] B. Buck, J.C. Johnston, A.C. Merchant, and S.M. Perez, Phys. Rev. **C53**, 2841 (1996) and references therein.
[13] A. Astier, P. Petkov, M.-G. Porquet, D.S. Delion, and P. Schuck, Phys. Rev. Lett. **104**, 042701 (2010).
[14] J. Simpson, Z. Phys. A**358**, 139 (1997).
[15] J. Eberth *et al.*, Nucl. Instr. Meth. A **369**, 135 (1996).
[16] G. Duchêne *et al.*, Nucl. Instr. Meth. A **432**, 90 (1999).
[17] M.-G. Porquet, Int. J. Mod. Phys. **E13**, 29 (2004).
[18] D.C. Radford, Nucl. Instr. Meth. Phys. Res. A **361**, 297 and 306 (1995).
[19] T. Yamazaki, Nucl. Data **A3**, 1 (1967).
[20] A. Astier *et al.*, Eur. Phys. J. **A 30**, 541 (2006) and references therein.
[21] P.M. Jones *et al.*, Nucl. Instr. Meth. Phys. Res. A **362**, 556 (1995).
[22] T.K. Alexander and J.S. Forster, Adv. Nucl. Phys. **10**, 197 (1978).
[23] G. Winter, ZfK Rossendorf Report ZfK-497, 1983.
[24] G. Winter, Nucl. Instr. Meth. **214**, 537 (1983).
[25] P. Petkov *et al.*, Nucl. Phys. **A640**, 293 (1998).
[26] F. Videbæk *et al.*, Phys. Rev C bf 15, 954 (1977).

[27] T. Kibédi *et al.*, Nucl. Instrum. Methods **A589**, 202 (2008), http://www.rsphysse.anu.edu.au/nuclear/bricc/.
[28] ENSDF data base, http://www.nndc.bnl.gov/ensdf/.
[29] E.L. Church and J. Weneser, Phys. Rev. **104**, 1382 (1956).
[30] T.A. Green and M.E. Rose, Phys. Rev. **110**, 105 (1958).
[31] S.V. Nilsson and J.O. Rasmussen, Nucl. Phys. **5**, 617 (1958).
[32] H.C. Pauli, K. Alder, and R.M. Steffen, in: *The electromagnetic interaction in nuclear spectroscopy*, ed. W.D. Hamilton, North-Holland, Amsterdam, 1975
[33] L.C. Northcliffe and R.F. Schilling, Nucl. Data Tables A7 (1970) 233.
[34] J.F. Ziegler and W.K. Chu, Atomic Data and Nucl. Data Tables 13 (1974) 463.
[35] J.F. Ziegler and J.P. Biersack, in *Treatise on Heavy-Ion Science*, vol. 6, ed. D.A. Bromley, (Plenum Press, 1985), p.95.
[36] J. Lindhard, M. Scharff and H.E. Schiøtt, Kgl. Dan. Vid. Selsk. Mat. Fys. Medd., 33, no. 14 (1963).
[37] W.M Currie, Nucl. Instr. Meth. **73** (1969) 173.
[38] J. Keinonen, in *Capture Gamma-Ray Spectroscopy and Related Topics-1984*, Proceedings of the Fifth International Symposium, Knoxville, Tennessee, AIP Conf. Proc. No. 125, ed. S. Raman, (AIP, New York, 1985), p. 557.
[39] P.A. Baidsen *et al.*, Phys. Rev. Lett. **41**, 738 (1978).
[40] R.M. Lieder *et al.*, Phys. Rev. Lett. **41**, 742 (1978).
[41] P. Lemmertz *et al.*, Zeit. Phys. A **298**, 311 (1980).
[42] K. Eskola *et al.*, Phys. Rev. C **29**, 2160 (1984).
[43] E. Browne, Nuclear Data Sheets **104**, 441 (2005).
[44] P. Ring, P. Schuck, *The Nuclear Many Body Problem*, Springer-Verlag, 1980.
[45] W. Satula, J. Dobaczewski and W. Nazarewicz, Phys. Rev. Lett. **81**, 3599 (1998).
[46] D. C. Radford et al., Nucl. Phys. **A752**, 264c (2005).
[47] J. Terasaki, J. Engel, W. Nazarewicz, and M. Stoitsov, Phys. Rev C **66**, 054313 (2002).
[48] A. Covello, L. Coraggio, A. Gargano and N. Itaco, Prog. Part. Nucl. Phys. **59**, 401 (2007).
[49] B. Buck, A.C. Merchant and S.M. Perez, Phys. Rev Lett. **65**, 2975 (1990).
[50] C. Qi, F.R. Xu, R.J. Liotta and R. Wyss, Phys. Rev. Lett. **103**, 072501 (2009) and references therein.
[51] M.A. Preston and R.K. Bhaduri, *Structure of the Nucleus*, chapter 11 (Addison-Wesley, 1975).
[52] C. Ellegard, P.D. Barnes, E.R. Flynn, and G.J. Igo, Nucl. Phys. **A162**, 1 (1971).
[53] G.D. Dracoulis *et al.*, Nucl. Phys. **A493**, 145 (1989).
[54] M. Piiparinen *et al.*, Zeit. Phys. **A337**, 387 (1990).
[55] Zs. Podolyak *et al.*, Eur. Phys. J. **A17**, 29 (2003).
[56] I. Ahmad and P. Butler, Ann. Rev. Nucl. Part. Sci. **43**, 71 (1993).
[57] P. Butler and W. Nazarewicz, Rev. Mod. Phys. **68**, 349 (1996).
[58] M. Gai *et al.*, Phys. Rev. C **43**, 2127 (1991).
[59] F. Iachello, Phys. Lett. **160B**, 1 (1985).
[60] E. Merzbacher, *Quantum Mechanics*, chapter 5 (John Wiley and Sons, 1961).
[61] W. von Oertzen, M. Freer and Y. Kanada-En'yo, Phys. Rep. **432**, 43 (2006).